*mathematics*

MDPI

*Article*

# Dynamic Analysis of Sigmoid Bidirectional FG Microbeams under Moving Load and Thermal Load: Analytical Laplace Solution

**Mohamed A. Attia [1], Ammar Melaibari [2], Rabab A. Shanab [3] and Mohamed A. Eltaher [2,*]**

[1] Mechanical Design and Production Department, Faculty of Engineering, Zagazig University, P.O. Box 44519, Zagazig 44519, Egypt
[2] Mechanical Engineering Department, Faculty of Engineering, King Abdulaziz University, Jeddah P.O. Box 80204, Saudi Arabia
[3] Engineering Mathematics Department, Faculty of Engineering, Zagazig University, P.O. Box 44519, Zagazig 44519, Egypt
* Correspondence: meltaher@kau.edu.sa or mohaeltaher@gmail.com; Tel.: +966-565518613 or +20-1001089561

**Abstract:** This paper presents for the first time a closed-form solution of the dynamic response of sigmoid bidirectional functionally graded (SBDFG) microbeams under moving harmonic load and thermal environmental conditions. The formulation is established in the context of the modified couple stress theory to integrate the effects of microstructure. On the basis of the elasticity theory, nonclassical governing equations are derived by using Hamilton's principle in combination with the parabolic higher-order shear deformation theory considering the physical neutral plane concept. Sigmoid distribution functions are used to describe the temperature-dependent thermomechanical material of bulk continuums of the beam in both the axial and thickness directions, and the gradation of the material length scale parameter is also considered. Linear and nonlinear temperature profiles are considered to present the environmental thermal loads. The Laplace transform is exploited for the first time to evaluate the closed-form solution of the proposed model for a simply supported (SS) boundary condition. The solution is verified by comparing the predicted fundamental frequency and dynamic response with the previously published results. A parametric study is conducted to explore the impacts of gradient indices in both directions, graded material length scale parameters, thermal loads, and moving speed of the acted load on the dynamic response of microbeams. The results can serve as a principle for evaluating the multi-functional and optimal design of microbeams acted upon by a moving load.

**Keywords:** closed-form solution; Laplace transform; sigmoid microbeams; dynamic response; moving load; couple stress; thermomechanical

**MSC:** 74H45

**Citation:** Attia, M.A.; Melaibari, A.; Shanab, R.A.; Eltaher, M.A. Dynamic Analysis of Sigmoid Bidirectional FG Microbeams under Moving Load and Thermal Load: Analytical Laplace Solution. *Mathematics* **2022**, *10*, 4797. https://doi.org/10.3390/math10244797

Academic Editor: Fernando Simoes

Received: 21 November 2022
Accepted: 14 December 2022
Published: 16 December 2022



## 1. Introduction

Functionally graded material (FGM) is an innovative class of composites with continuous gradation of material through a certain spatial direction, which have enhanced properties rather than traditional composites, such as designability, reduced singular stress interface problems, small stress concentration, lower weight, higher fracture toughness, enhanced thermal properties, high damage resistance, etc. [1]. Due to their unique properties, FGMs are broadly employed in many applications such as electronics, dental implants, and turbines, as well as in aerospace, marine, automotive, military, and nuclear applications [2,3]. Due to the rapid advances in nanotechnology, FGMs nowadays are exploited in micro/nano-electro-mechanical systems (MEMs/NEMs), atomic force

microscopes, shape memory alloys, thin film coatings, and transmission systems [4,5]. At nanometer scales, size effects, which are missing in classical mechanics, often become important and observable and must be considered in the analysis and design of MEMs/NEMs [6]. To consider a size effect, modified continuum models such as nonlocal theories, modified couple stress theory, strain gradient theory, nonlocal strain gradient, doublet mechanics, and surface energy are exploited [7].

Asghari et al. [8] analytically studied the mechanical responses of FG-modified couple stress nanobeams based on first-order shear deformation theory (FOSDT). Şimşek [9] evaluated the critical buckling loads of 2d-FG Timoshenko beams with different boundary conditions via the Ritz method. Nejad et al. [10,11] examined the buckling stability and free vibration of arbitrary 2D-FG thin nonlocal nanobeams by using the generalized differential quadrature method. Mirafzal and Fereidoon [12] investigated the vibration behaviors of temperature-dependent viscoelastic FG nonlocal nanobeams exposed to a 2D-magnetic field under periodic loading. Shafiei et al. [13,14] studied buckling and vibration behaviors of 2D-FG porous tapered modified couple stress nanoscale beams using Euler and Timoshenko beam theories. Rajasekaran and Khaniki [15] illustrated the impact of single/multi-cracked 2D-FG beams on free vibration by using a novel finite element method. Sahmani and Safaei [16,17] investigated the nonlinear vibrations of 2D-FG nonlocal strain gradient micro/nanobeams within the framework of the refined hyperbolic shear deformation beam theory. Tang and Ding [18] studied the nonlinear hygro-thermal dynamics of 2D-FG beams with coupled transverse and longitudinal displacements. Tang et al. [19] presented the asymmetric mode and nonlinear vibration of 2D-FG Euler–Bernoulli beams via the homotopy analysis method. Attia and Mohamed [20] studied the nonlinear vibration characteristics of pre- and postbuckled nonuniform 2D-FGM-modified couple stress microbeams exposed to nonlinear thermal loading.

Barati et al. [21] evaluated the natural frequencies of 2D-FGM nonlocal nanobeam under a magnetic field employed by Maxwell's relations. Ghatage et al. [22] presented a comprehensive review on the modeling and mechanical analysis of multi-directional FG beam, plate, and shell structures. Karami et al. [23] studied the dynamic response of 2D-FG-tapered Timoshenko nonlocal strain gradient nanobeams in a thermal environment by using the numerical generalized differential quadrature method. Zhao et al. [3] examined buckling and postbuckling of FG graphene origami (GOri)-enabled auxetic metallic metamaterial (GOEAM) beams. Guo et al. [24] examined the elastic wave dispersion propagating along the thickness direction in FG-laminated phononic crystal auxetic metamaterials. Zhao et al. [25] proposed data-driven micromechanics models based on molecular dynamic (MD) simulations to predict thermo-elastic properties of vacancy-defective graphene/Cu nanocomposites in different temperature conditions. Daikh et al. [26] studied bending and stress responses of nonlocal strain gradient Quasi-3D FG sandwich nanoplates based on the sigmoid gradation function. Daikh et al. [27] explored the static buckling stability, static deflection, and vibration of an axially temperature-dependent FG-CNTs nanoplate based on higher-order shear deformation. Soni et al. [28] presented an extensive review on FG carbon nanotube-reinforced composite structures, their application, and studies on the mechanical, vibration, thermal, thermo-mechanical, and low-velocity impact responses. Ahmadi [6] exploited the meshless method to examine the dynamic response of 2D-FG nonlocal nanobeams by using FOSDT. Attia and Shanab [29] investigated the size-dependent bending, buckling, and vibration responses of 2D-FG micro/nanoscale beams including the microstructure surface energy-based theory. Zhao et al. [30] presented a comprehensive review on the mechanical analyses of FG graphene platelet-reinforced composite structure. Assie et al. [31] studied the buckling stability of BDFG porous plates resting on an elastic foundation by using unified higher-order shear theories.

Understanding the dynamic motion of nanoparticles is critical for MEMS/NEMS and microfluidics [32]. For example, in biological and colloidal science applications, nanotubes and nanobeams are exploited to transport drug materials into targeted nano-sized

molecules to change the behavior of cancer cells [33]. Therefore, understanding the process of mass transport and the dynamic response of micro/nanobeams under such loadings would be of great importance for optimal designs [34]. Şimşek [35] analytically studied the forced vibration of an elastically connected double-carbon nanotube system (DCNTS) under a moving nanoparticle. Şimşek [36] investigated the forced vibration of a simply supported (SS) single-walled carbon nanotube (SWCNT) under a moving harmonic load, based on nonlocal Euler–Bernoulli beam theory, and showed that dynamic deflection of the SWCNT is strongly affected by the nonlocal parameter, and that its dynamic behavior is also affected by other parameters such as load velocity and excitation frequency. Şimşek [9] developed a mathematical model to examine free and forced vibration of 2D-FG Timoshenko beams under moving loads with the implicit Newmark time integration method. Hosseini and Rahmani [37] adopted the nonlocal elasticity theory to study the dynamic response of SS-FG Euler–Bernoulli nanobeams subjected to a constant moving load. Based on nonlocal elasticity theory, the influences of surface energy and viscoelastic foundation on the steady-state response of Euler–Bernoulli nanobeams in a thermal environment and subjected to a moving concentrated load were examined by Ghadiri et al. [38] using the multiple scales method. In Barati and Shahverdi [39], the forced vibration response of FG nanobeams resting on Winkler–Pasternak foundation and under a uniform harmonic dynamic load was investigated employing a higher-order shear deformation beam theory in the context of nonlocal elasticity theory. In the framework of parabolic shear deformation theory, Zhang and Liu [40] employed the modified couple stress theory to study the vibration response of 2D-FG porous microbeams excited by a moving harmonic load using FEM.

For even and uneven porosity distributions, power law functions were adopted to model the material variation in both thickness and length directions. Liu et al. [41] adopted the modified couple stress theory to explore the effects of thermal rise and moving load on the vibration response of 2D-FG microbeams using FEM. Temperature-dependent material properties were assumed with a power law distribution in both the thickness and length directions. Hosseini et al. [42] presented the influence of the thermal environment on the forced vibration response of FG nonlocal nanobeams under moving load via the Laplace transform method. Abdelrahman et al. [43–45] analyzed the dynamic response of perforated nanobeams and FG nanobeams reinforced by carbon nanotubes under moving load via nonlocal strain gradient. Chung et al. [46] developed a new type of planar transmission line with unique dual-signal path characteristics and ultimately achieved circuit miniaturization. Eltaher et al. [47] exploited bottom-up modeling nanomechanics theory to illustrate the dynamic response of armchair and zigzag CNTs under a dynamic moving load. Esen et al. [48,49] exploited nonlocal strain gradient theory to present the size scale and microstructure effects on the dynamic response of FG nanobeams reinforced by carbon nanotubes and sigmoid FG nanobeams under moving loads. Thongchom et al. [50] studied the vibration behavior of fluid-conveying hybrid smart CNTs considering slip boundary conditions under a moving nanoparticle. Akbaş et al. [51] studied the dynamic responses of a fiber-reinforced composite Timoshenko beam under a moving load by using the Ritz method.

Based on the literature and our knowledge, the dynamic analysis of sigmoid BDFG microbeams with temperature-dependent materials under moving and thermal loads appears limited. Thus, this article aims to fill this gap analytically by using Laplace transform on a system of variable coefficients for the first time. The effect of microstructure is captured via the modified couple stress. The materials' compositions are changing gradually through thickness and length by sigmoidal functions. The formulation considers the physical neutral axis concept. The nonclassical motion equations are derived. Laplace transform and the Newmark method are employed to evaluate the dynamic deflection of BDFG microbeams under moving loads. The rest of the article is organized as follows. The formulation, constitutive equations, distribution functions, and kinematic relations are presented in Section 2. The variational techniques to derive the equations of motion and the

boundary conditions are given in Section 3. Analytical solutions and model validation are presented in Sections 4 and 5, respectively. Numerical and parametric studies to present the influence of gradation, temperature distribution, and moving velocity on the dynamic response are discussed in Section 6.

## 2. Theory and Formulation

### *2.1. Material Constitutions and Distributions*

Consider a straight uniform sigmoid bidirectional functionally graded (SBDFG) microbeam with $b$ width, $L$ length, and $h$ thickness, as shown in Figure 1, in a Cartesian system ($x_m$, $y$, $z_m$) that represents the midplane. The beam is excited by a moving load with a constant velocity $v$. The FG beam is composed of a mixture of ceramic and metallic constituents, where the lowermost ($x = 0$, $z_m = -\frac{h}{2}$) is pure metal "$m$" and the uppermost ($x = L$, $z_m = \frac{h}{2}$) is pure ceramic "$c$". The equivalent thermomechanical properties for the bulk continuum of SBDFG at temperature $T(z)$ can be described by a sigmoid function in both directions as [52]:

$$\mathcal{P}_1(x,z,T) = \left\{\mathcal{P}_m(T) + \left(\mathcal{P}_c(T) - \mathcal{P}_m(T)\right)\left[0.5\left(1+\frac{2z}{h}\right)^{k_z}\right]\left(\frac{x}{L}\right)^{k_x}\right\} \qquad -\frac{h}{2} \le z \le 0 \tag{1}$$

$$\mathcal{P}_2(x,z,T) = \left\{\mathcal{P}_m(T) + \left(\mathcal{P}_c(T) - \mathcal{P}_m(T)\right)\left[1-0.5\left(1-\frac{2z}{h}\right)^{k_z}\right]\left(\frac{x}{L}\right)^{k_x}\right\} \qquad 0 \le z \le \frac{h}{2} \tag{2}$$

where $\mathcal{P}_m$ and $\mathcal{P}_c$ are the metallic and ceramic constituent properties, respectively. The material property "$\mathcal{P}$" represents the Young's modulus $E$, Poisson's ratio $\nu$, the mass density $\rho$, microstructure material length scale parameter (MSLSP) $l$, and thermal expansion coefficient $\alpha$. $k_x$ and $k_z$ are the gradient indices in the axial and transverse directions, respectively.

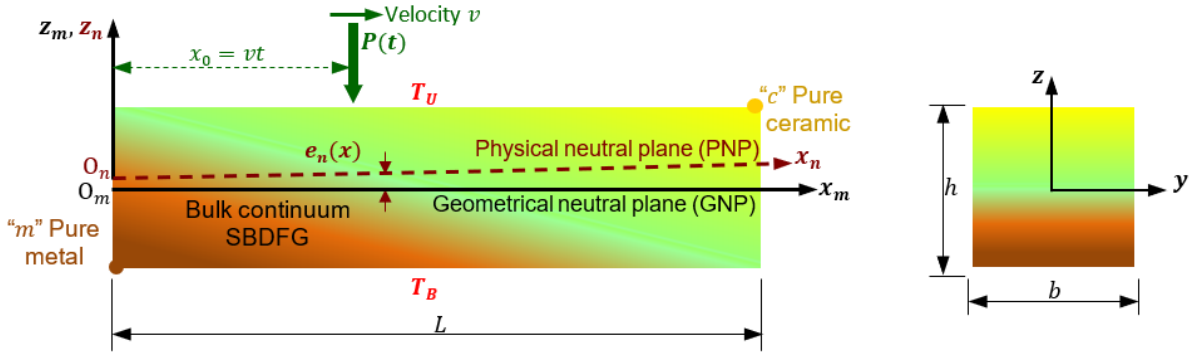


**Figure 1.** Illustration of a 2D-FG microbeam exposed to a moving load and thermal environment.

Lame's parameters of bulk are:

$$\lambda(x,z) = \frac{E(x,z_m)\,\nu(x,z_m)}{\left(1+\nu(x,z_m)\right)\left(1-2\nu(x,z_m)\right)} \quad \text{and} \quad \mu(x,z_m) = \frac{E(x,z_m)}{2\left(1+\nu(x,z_m)\right)} \tag{3}$$

Ignoring the Poisson effect yields, $[\lambda(x,z_m) + 2\mu(x,z_m)] \equiv E(x,z)$, as adopted by [53–55]. In Equations (1)–(3), the axially FG (AFG) and transversely FG (TFG) gradations can be obtained by setting $k_z = 0$ and $k_x = 0$, respectively. A pure metal constituent beam is obtained when $k_x = k_z = 0$. In addition, for $k_z = 1$, the power law distribution function is retained from Equations (1) and (2).

Temperature-dependent (TD) material properties $\mathcal{P}_m$ and $\mathcal{P}_c$ are estimated by [56]:

$$\mathcal{P}_i(T) = \mathcal{P}_0[\mathcal{P}_{-1}T^{-1} + 1 + \mathcal{P}_1 T + \mathcal{P}_2 T^2 + \mathcal{P}_3 T^3], i = m, c \tag{4}$$

where $\mathcal{P}_{-1}$, $\mathcal{P}_0$, $\mathcal{P}_1$, $\mathcal{P}_2$, and $\mathcal{P}_3$ are temperature-dependent coefficients.

Because of nonsymmetric material properties' gradation of the BDFG beam about its midplane, the geometrical neutral plane (GNP) does not coincide with the physical neutral plane (PNP) [57,58], as shown in Figure 1. The difference between the locations of GNP and PNP is evaluated by [29,59]:

$$e_n(x) = \frac{\int_{-\frac{h}{2}}^{\frac{h}{2}} \int_{-\frac{b}{2}}^{\frac{b}{2}} z_m \left[\lambda^B(x, z_m) + 2\mu^B(x, z_m)\right] \, dy \, dz_m}{\int_{-\frac{h}{2}}^{\frac{h}{2}} \int_{-\frac{b}{2}}^{\frac{b}{2}} \left[\lambda^B(x, z_m) + 2\mu^B(x, z_m)\right] \, dy \, dz_m}, \quad z_n(x) = z_m - e_n(x) \tag{5}$$

*2.2. Kinematics Relation*

Based on general shear deformation theory, the displacement field of the BDFG microbeam is presented by [60]:

$$\begin{aligned} u_x(x, z, t) &= u(x) + f(z_n)\frac{\partial w(x,t)}{\partial x} + R(z_n)\phi(x,t) \\ u_y(x, z, t) &= 0 \\ u_z(x, z, t) &= w(x,t) \end{aligned} \tag{6}$$

where $u$ and $w$ are the displacement components along the midplane, $\phi$ is the transverse shear function, and $t$ indicates time. The shear–strain function $R(z_n) = R(z_m) - r_n(x)$, where:

$$r_n(x) = \frac{\int_{-\frac{h}{2}}^{\frac{h}{2}} \int_{-\frac{b}{2}}^{\frac{b}{2}} R(z_m) \left[\lambda^B(x, z_m) + 2\mu^B(x, z_m)\right] \, dy \, dz_m}{\int_{-\frac{h}{2}}^{\frac{h}{2}} \int_{-\frac{b}{2}}^{\frac{b}{2}} \left[\lambda^B(x, z_m) + 2\mu^B(x, z_m)\right] \, dy \, dz_m} \tag{7}$$

Various beam theories can be derived by proper functions of $f(z_n)$ and $R(z_n)$. The Euler–Bernoulli and Timoshenko beam theories are achieved by setting $f(z_n) = -z_n$, $R(z_m) = 0$ and $f(z_n) = 0$, $R(z_m) = -z_m$, respectively. Adopting the third-order parabolic shear deformable beam theory (PSDBT) [61], we obtain:

$$f(z_n) = -z_n \quad \text{and} \quad R(z_m) = z_m\left(1 - \frac{4z_m^2}{3h^2}\right) \tag{8}$$

*2.3. Constitutive Relations*

Based on generalized elasticity theory and modified couple stress theory [62], the strain $\varepsilon$, Cauchy stress $\sigma^B$, symmetric curvature $\chi$, and the couple stress $m$ are given by [63,64]:

$$\varepsilon = \frac{1}{2}[\nabla \mathrm{u} + (\nabla \mathrm{u})^T] \tag{9}$$

$$\sigma^B = \lambda^B(x, z_m)\,\mathrm{tr}(\varepsilon) I + 2\mu^B(x, z_m)\,\varepsilon \tag{10}$$

$$\chi = \frac{1}{2}[\nabla \theta + (\nabla \theta)^T], \qquad \theta = \frac{1}{2}\mathrm{curl}(\mathrm{u}) \tag{11}$$

$$m = [2l^2(x, z_m)\mu^B(x, z_m)]\chi \tag{12}$$

where u and θ represent the displacement and rotation vectors, respectively. In this analysis, the gradation of the MLSP in thickness and length directions is considered, as described in Equations (1) and (2). The strain and the symmetric curvature components according to Equations (6), (8), (9) and (11) are:

$$\varepsilon_{xx} = \frac{\partial u}{\partial x} - z_n \frac{\partial^2 w}{\partial^2 x} + R(z_n)\frac{\partial \phi}{\partial x}$$
$$\gamma_{xz} = \gamma_{zx} = 2\varepsilon_{xz} = \frac{\partial R(z_n)}{\partial z_m}\phi \tag{13}$$

$$\chi_{xy} = \chi_{yx} = \frac{1}{2}\left(\frac{1}{2}\frac{\partial R(z_n)}{\partial z_m}\frac{\partial \phi}{\partial x} - \frac{\partial^2 w}{\partial x^2}\right)$$
$$\chi_{yz} = \chi_{zy} = \frac{1}{4}\frac{\partial^2 R(z_n)}{\partial z_m^2}\phi \tag{14}$$

According to Equations (8) and (13), the nonzero components of the classical Cauchy stress tensors including the thermal effects and the deviatoric part of the couple stress tensor are:

$$\sigma_{xx}^B = \mathbb{E}^B(x, z_m, T)\varepsilon_{xx} - \mathbb{E}^{th}(x, z_m, T)\,\varepsilon^{th} \tag{15}$$

$$\sigma_{xz}^B = \mu^B(x, z_m, T)\frac{\partial R(z_n)}{\partial z_m}\,\phi \tag{16}$$

$$m_{yx} = m_{xy} = 2[l^2(x, z_m)\,\mu^B(x, z_m)]\,\chi_{xy} \tag{17}$$

$$m_{zy} = m_{yz} = 2[l^2(x, z_m)\,\mu^B(x, z_m)]\,\chi_{zy} \tag{18}$$

where the equivalent elasticity and thermal moduli are [65]:

$$\mathbb{E}^B(x, z_m, T) = [\lambda^B(x, z_m, T) + 2\mu^B(x, z_m, T)] \tag{19}$$

$$\mathbb{E}^{th}(x, z_m, T) = [3\lambda^B(x, z_m, T) + 2\mu^B(x, z_m, T)] \tag{20}$$

By ignoring the influence of Poisson's ratio, Equations (19) and (20) can be simplified to:

$$\mathbb{E}^B(x, z_m, T) = \mathbb{E}^{th}(x, z_m, T) = E(x, z_m, T) \tag{21}$$

where $\varepsilon^{th} = \alpha(x, z_m, T)\,\Delta T(z)$, which presents the thermal strain induced by temperature rise $\Delta T$ from the ambient temperature $T_0$, and $\alpha$ is the thermal expansion coefficient.

## 3. Formulation of Governing Equations

Based on elasticity theory and modified couple stress theory, the total strain energy ($\mathbb{U}$) of the BDFG beam is [66–68]:

$$\mathbb{U} = \frac{1}{2}\int_0^L \int_A \left[\sigma_{ij}\varepsilon_{ij} + m_{ij}\chi_{ij}\right] dA dx \tag{22}$$

where $A$ is the cross-sectional area. Substituting Equations (15)–(18) into Equation (22) produces:

$$\mathbb{U} = \frac{1}{2}\delta\int_0^L \int_A \sigma_{xx}\varepsilon_{xx} + 2\sigma_{xz}\varepsilon_{xz} + 2m_{xy}\chi_{xy} + 2m_{yz}\chi_{yz}\, dA dx \tag{23}$$

Substituting Equations (15)–(18), the first variation of Equation (23) can be obtained as:

$$\delta\mathbb{U} = \int_0^L \left\{N(x)\frac{\partial \delta u}{\partial x} - [M_c(x) + \mathrm{Y}_1(x)]\frac{\partial^2 \delta w}{\partial x^2} + \left[M_{nc}(x) + \frac{1}{2}\mathrm{Y}_2(x)\right]\frac{\partial \delta\phi}{\partial x} + \left[Q_{nc}(x) + \frac{1}{2}\mathrm{Y}_3(x)\right]\delta\phi\right\} dx dt \tag{24}$$

The classical Cauchy stress and couple stress resultants of the bulk continuum can be obtained as:

$$\begin{Bmatrix} N(x) \\ M_c(x) \\ M_{nc}(x) \end{Bmatrix} \equiv \int_A \sigma_{xx} \begin{Bmatrix} 1 \\ z_n \\ R(z_n) \end{Bmatrix} dA = \begin{bmatrix} A_{xx}(x) & B_{xx}(x) & E_{xx}(x) \\ B_{xx}(x) & D_{xx}(x) & F_{xx}(x) \\ E_{xx}(x) & F_{xx}(x) & H_{xx}(x) \end{bmatrix} \begin{Bmatrix} \dfrac{\partial u}{\partial x} \\ -\dfrac{\partial^2 w}{\partial x^2} \\ \dfrac{\partial \phi}{\partial x} \end{Bmatrix} \tag{25}$$

$$Q_{nc}(x) = \int_A \frac{dR(z_n)}{dz_m} \sigma_{xz}\, dA \equiv \bar{B}_{xz}(x)\phi \tag{26}$$

$$\begin{Bmatrix} \mathrm{Y}_1(x) \\ \mathrm{Y}_2(x) \\ \mathrm{Y}_3(x) \end{Bmatrix} \equiv \int_A m_{xy} \begin{Bmatrix} 1 \\ \dfrac{dR(z_n)}{dz} \\ \dfrac{d^2R(z_n)}{dz^2} \end{Bmatrix} dA = \begin{bmatrix} A_{xz}(x) & 0 & \dfrac{1}{2}D_{xz}(x) \\ D_{xz}(x) & 0 & \dfrac{1}{2}B_{xz}(x) \\ 0 & \dfrac{1}{2}E_{xz}(x) & 0 \end{bmatrix} \begin{Bmatrix} -\dfrac{\partial^2 w}{\partial x^2} \\ \phi \\ \dfrac{\partial \phi}{\partial x} \end{Bmatrix} \tag{27}$$

with

$$\begin{Bmatrix} A_{xx}(x) \\ B_{xx}(x) \\ D_{xx}(x) \\ E_{xx}(x) \\ F_{xx}(x) \\ H_{xx}(x) \end{Bmatrix} = \int_{-\frac{b}{2}}^{\frac{b}{2}} \int_{-\frac{h}{2}}^{\frac{h}{2}} \mathbb{E}(x, z_m, T) \begin{Bmatrix} 1 \\ z_n \\ z_n^2 \\ R(z_n) \\ z_n R(z_n) \\ R^2(z_n) \end{Bmatrix} dzdy \tag{28}$$

$$\bar{B}_{xz}(x) = \int_{-\frac{b}{2}}^{\frac{b}{2}} \int_{-\frac{h}{2}}^{\frac{h}{2}} \mu(x, z_m, T) \left( \frac{\partial R(z_n)}{\partial z} \right)^2 dzdy \tag{29}$$

$$\begin{Bmatrix} A_{xz}(x) \\ B_{xz}(x) \\ D_{xz}(x) \\ E_{xz}(x) \end{Bmatrix} \equiv \int_{-\frac{b}{2}}^{\frac{b}{2}} \int_{-\frac{h}{2}}^{\frac{h}{2}} [l^2(x, z_m)\, \mu(x, z_m, T)] \begin{Bmatrix} 1 \\ \left( \dfrac{\partial R(z_n)}{\partial z} \right)^2 \\ \dfrac{\partial R(z_n)}{\partial z} \\ \left( \dfrac{\partial^2 R(z_n)}{\partial z^2} \right)^2 \end{Bmatrix} dzdy \tag{30}$$

Performing the partial integration in Equation (17) with respect to $x$ and $t$ over the time interval $[t_0, t_f]$, the total strain energy first variation can be calculated as:

$$\begin{aligned} \int_{t_0}^{t_f} \delta \mathbb{U}\, dt \equiv & -\int_{t_0}^{t_f} \int_0^L \left\{ \left[ \frac{\partial \boldsymbol{\mathcal{N}}_{xx}(x)}{\partial x} \right] \delta u + \left[ \frac{\partial^2 \boldsymbol{\mathcal{M}}_w(x)}{\partial x^2} \right] \delta w + \left[ \frac{\partial \boldsymbol{\mathcal{M}}_\phi(x)}{\partial x} - \boldsymbol{\mathcal{Q}}_\phi(x) \right] \delta \phi \right\} dxdt \\ & + \int_{t_0}^{t_f} \left\{ [\boldsymbol{\mathcal{N}}_{xx}(x)] \delta u + \left[ \frac{\partial \boldsymbol{\mathcal{M}}_w(x)}{\partial x} \right] \delta w - [\boldsymbol{\mathcal{M}}_w(x)] \frac{\partial \delta w}{\partial x} + [\boldsymbol{\mathcal{M}}_\phi(x)] \delta \phi \right\}_0^L dt \end{aligned} \tag{31}$$

in which the effective stress resultants are defined as

$$\begin{Bmatrix} N^B(x) \\ M_c^B(x) \\ M_{nc}^B(x) \end{Bmatrix} \equiv \int_A \sigma_{xx} \begin{Bmatrix} 1 \\ z_n \\ R(z_n) \end{Bmatrix} dA = \begin{bmatrix} A_{xx}^B(x) & B_{xx}^B(x) & E_{xx}^B(x) \\ B_{xx}^B(x) & D_{xx}^B(x) & F_{xx}^B(x) \\ E_{xx}^B(x) & F_{xx}^B(x) & H_{xx}^B(x) \end{bmatrix} \begin{Bmatrix} \dfrac{\partial u}{\partial x} \\ -\dfrac{\partial^2 w}{\partial x^2} \\ \dfrac{\partial \phi}{\partial x} \end{Bmatrix} \tag{32}$$

$$\begin{Bmatrix} \mathrm{Y}_1^B(x) \\ \mathrm{Y}_2^B(x) \\ \mathrm{Y}_3^B(x) \end{Bmatrix} \equiv \int_A m_{xy} \begin{Bmatrix} 1 \\ \dfrac{dR(z_n)}{dz} \\ \dfrac{d^2R(z_n)}{dz^2} \end{Bmatrix} dA = \begin{bmatrix} A_{xz}(x) & 0 & \dfrac{1}{2}D_{xz}(x) \\ D_{xz}(x) & 0 & \dfrac{1}{2}B_{xz}(x) \\ 0 & \dfrac{1}{2}E_{xz}(x) & 0 \end{bmatrix} \begin{Bmatrix} -\dfrac{\partial^2 w}{\partial x^2} \\ \phi \\ \dfrac{\partial \phi}{\partial x} \end{Bmatrix} \tag{33}$$

and

$$\begin{Bmatrix} \boldsymbol{\mathcal{N}}(x) \\ \boldsymbol{\mathcal{M}}_c(x) \\ \boldsymbol{\mathcal{M}}_{nc}(x) \end{Bmatrix} = \begin{Bmatrix} \boldsymbol{\mathcal{N}}_{xx}(x) \\ \boldsymbol{\mathcal{M}}_w(x) \\ \boldsymbol{\mathcal{M}}_\phi(x) \end{Bmatrix} \equiv \begin{Bmatrix} N^B(x) \\ M_c^B(x) + \mathrm{Y}_1^B(x) \\ M_{nc}^B(x) + \dfrac{1}{2}\mathrm{Y}_2^B(x) \end{Bmatrix} = \begin{bmatrix} \mathrm{A}_{11}(x) & \mathrm{B}_{11}(x) & \mathrm{E}_{11}(x) \\ \mathcal{B}_{11}(x) & \mathcal{D}_{11}(x) & \mathcal{F}_{11}(x) \\ \mathcal{E}_{11}(x) & \mathcal{F}_{11}(x) & \mathcal{H}_{11}(x) \end{bmatrix} \begin{Bmatrix} \dfrac{\partial u}{\partial x} \\ -\dfrac{\partial^2 w}{\partial x^2} \\ \dfrac{\partial \phi}{\partial x} \end{Bmatrix} \tag{34}$$

$$\boldsymbol{\mathcal{Q}}(x) = \boldsymbol{\mathcal{Q}}_\phi \equiv Q_{nc}(x) + \frac{1}{2}\mathrm{Y}_3^B(x) = \mathcal{B}_{xz}(x)\phi \tag{35}$$

with

$$\begin{Bmatrix} \mathcal{A}_{11}(x) \\ \mathcal{B}_{11}(x) \\ \mathcal{D}_{11}(x) \\ \mathcal{E}_{11}(x) \\ \mathcal{F}_{11}(x) \\ \mathcal{H}_{11}(x) \\ \mathcal{B}_{xz}(x) \end{Bmatrix} = \begin{Bmatrix} A_{xx}^B(x) \\ B_{xx}^B(x) \\ D_{xx}^B(x) + A_{xz}(x) \\ E_{xx}^B(x) \\ F_{xx}^B(x) + \dfrac{1}{2}D_{xz}(x) \\ H_{xx}^B(x) + \dfrac{1}{4}B_{xz}(x) \\ \bar{B}_{xz}(x) + \dfrac{1}{4}E_{xz}(x) \end{Bmatrix} \tag{36}$$

The kinetic energy of 2D-FG microbeams accounting for the size effect can be expressed as:

$$\begin{aligned} \mathbb{T} \equiv \frac{1}{2}\int_0^L \int_A \rho^B(x, z_m, T)\left[\left(\frac{\partial u_x}{\partial t}\right)^2 + \left(\frac{\partial u_z}{\partial t}\right)^2\right] dA dx \\ = \frac{1}{2}\int_0^L \left[\left(\mathrm{I}_A(x)\frac{\partial u}{\partial t} - \mathrm{I}_B(x)\frac{\partial^2 w}{\partial x \partial t} + \mathrm{I}_E(x)\frac{\partial \phi}{\partial t}\right)\frac{\partial u}{\partial t} + \mathrm{I}_\mathrm{A}(x)\left(\frac{\partial w}{\partial t}\right)\frac{\partial w}{\partial t}\right. \\ \left. - \left(\mathrm{I}_B(x)\frac{\partial u}{\partial t} - \mathrm{I}_D(x)\frac{\partial^2 w}{\partial x \partial t} + \mathrm{I}_F(x)\frac{\partial \phi}{\partial t}\right)\frac{\partial^2 w}{\partial x \partial t} + \left(\mathrm{I}_E(x)\frac{\partial u}{\partial t} - \mathrm{I}_F(x)\frac{\partial^2 w}{\partial x \partial t} + \mathrm{I}_H(x)\frac{\partial \phi}{\partial t}\right)\frac{\partial \phi}{\partial t}\right] dx \end{aligned} \tag{37}$$

where the mass moments of inertia are computed by

$$\begin{Bmatrix} \mathrm{I}_A(x) \\ \mathrm{I}_B(x) \\ \mathrm{I}_D(x) \\ \mathrm{I}_E(x) \\ \mathrm{I}_F(x) \\ \mathrm{I}_H(x) \end{Bmatrix} = \int_{-\frac{b}{2}}^{\frac{b}{2}} \int_{-\frac{h}{2}}^{\frac{h}{2}} \rho^B(x, z_m, T) \begin{Bmatrix} 1 \\ z_n \\ z_n^2 \\ R(z_n) \\ z_n R(z_n) \\ R^2(z_n) \end{Bmatrix} dzdy \tag{38}$$

The first-order variation of the kinetic energy of BDFG microbeam can be expressed by:

$$\delta\mathbb{T} = \int_{t_0}^{t_f} \int_0^L \left[ \mathbb{p}_u(x) \frac{\partial \delta u}{\partial t} + \mathbb{p}_w(x) \frac{\partial \delta w}{\partial t} + \mathbb{p}_{w2}(x) \frac{\partial^2 \delta w}{\partial x \partial t} + \mathbb{p}_\phi(x) \frac{\partial \delta \phi}{\partial t} \right] dxdt \tag{39}$$

in which the momentums are

$$\begin{Bmatrix} \mathbb{p}_u(x) \\ \mathbb{p}_w(x) \\ \mathbb{p}_{w2}(x) \\ \mathbb{p}_\phi(x) \end{Bmatrix} = \begin{bmatrix} \mathrm{I}_A(x) & 0 & -\mathrm{I}_B(x) & \mathrm{I}_E(x) \\ 0 & \mathrm{I}_A(x) & 0 & 0 \\ -\mathrm{I}_B(x) & 0 & \mathrm{I}_D(x) & 0 \\ \mathrm{I}_E(x) & 0 & -\mathrm{I}_F(x) & \mathrm{I}_H(x) \end{bmatrix} \begin{Bmatrix} \frac{\partial u}{\partial t} \\ \frac{\partial w}{\partial t} \\ \frac{\partial^2 w}{\partial x \partial t} \\ \frac{\partial \phi}{\partial t} \end{Bmatrix} \tag{40}$$

Proceeding the above integration by parts over the time interval $[t_0, t_f]$ with respect to $x$ and $t$, and using the zero variation at time boundaries ($t = t_0$ and $t = t_f$), we obtain the following:

$$\begin{aligned} \int_{t_0}^{t_f} \delta\mathbb{T}\, dt \equiv & - \int_{t_0}^{t_f} \int_0^L \left[ \left\{ \frac{\partial \mathbb{p}_u(x)}{\partial t} \right\} \delta u + \left\{ \frac{\partial \mathbb{p}_{w1}(x)}{\partial t} - \frac{\partial^2 \mathbb{p}_{w2}(x)}{\partial x \partial t} \right\} \delta w + \left\{ \frac{\partial \mathbb{p}_\phi(x)}{\partial t} \right\} \delta \phi \right] dxdt + \int_{t_0}^{t_f} \left[ \left\{ -\frac{\partial \mathbb{p}_{w2}(x)}{\partial t} \right\} \delta w \right]_0^L dt \\ & + \int_0^L \left[ \{\mathbb{p}_u(x)\} \delta u + \{\mathbb{p}_w(x)\} \delta w + \{\mathbb{p}_{w2}(x)\} \frac{\partial \delta w}{\partial x} + \{\mathbb{p}_\phi(x)\} \delta \phi \right]_{t_0}^{t_f} dx \end{aligned} \tag{41}$$

### *3.1. Moving Load Formulations*

The virtual work carried out by the applied forces on the BDFG beam, including modified couple stress theory, can be expressed as:

$$\delta\mathbb{W} = \int_\Omega (\mathbf{f} \cdot \delta \boldsymbol{u} + \mathbf{f}_c \cdot \delta \boldsymbol{\theta}) d\Omega + \oint_{\partial A} (\bar{\mathbf{t}} \,.\, \delta \mathbf{u} + \bar{\mathbf{s}} \,.\, \delta \boldsymbol{\theta}) dS \tag{42}$$

where $\mathbf{f}$ is the body force resultant and $\mathbf{f}_c$ is the body couple resultant per unit volume. In the absence of an applied compressive force, assuming the externally applied harmonic load moves with a constant speed, ignoring its inertial effect, a uniform thermal environment is assumed, and employing zero initial conditions, the virtual work in the time interval $[t_0, t_f]$ can be obtained as:

$$\begin{aligned} \int_{t_0}^{t_f} \delta\mathbb{W}\, dt = & \int_0^L \left\{ f_u \delta u + \left[ P(x)\delta(x - vt) + q + \frac{\partial}{\partial x}\left( f_c - \frac{1}{2} f_c a_c(x) \right) \right] \delta w - \left( \frac{1}{2} f_c a_c(x) + N_{th} \frac{\partial \mathrm{w}}{\partial \mathrm{x}} \right) \delta \frac{\partial w}{\partial x} + \left( \frac{1}{2} f_c a_c(x) \right) \delta \phi \right\} dx \\ & + \int_{t_0}^{t_f} \left\{ \bar{N} \delta u + \left[ \bar{V} - \left( f_c - \frac{1}{2} f_c a_c(x) \right) \right] \delta w - (\bar{M}_c + \bar{M}_{nc}) \delta \frac{\partial w}{\partial x} - \bar{M}_c \delta \phi \right\}_0^L dt \end{aligned} \tag{43}$$

where $\delta$ is the Dirac delta function, and $f_u$ and $q$ are distributed loads in the $x$- and $z$-directions, respectively. $f_c$ represents the $y$-component of the body couple per unit

length along the $x$-axis. $\bar{N}$ is applied axial force, $\bar{V}$ is applied lateral force, $\bar{M}_c$ is the classical bending moment, $\bar{M}_{nc}$ is the nonclassical bending moment due to the couple stress, and $a_c$ is defined as:

$$a_c(x) = \int_{-b/2}^{b/2} \int_{-h/2}^{h/2} \frac{\partial R(z_n)}{\partial z} \, dzdy \tag{44}$$

The applied external moving harmonic load is given by:

$$P(x) = P_0 \sin \Omega t \tag{45}$$

in which $P_0$ and $\Omega$ are the amplitude and frequency, respectively, of the applied moving load.

*3.2. Thermal Environment Formulations*

To consider the impact of the thermal environment on the microbeam, a nonlinear temperature profile can be described by [65]:

$$T(z) = T_0 + \Delta T \left(\frac{z}{h} + \frac{1}{2}\right)^{\alpha_T} \tag{46}$$

where the temperature difference $\Delta T = T_U - T_0$, and the lower surface temperature is kept constant at $T_B = T_0$.

Based on the power index $\alpha_T$, two different temperature profiles across the thickness of the beam can be evaluated:

- Linear temperature rise (LTR) for $\alpha_T = 1$;
- Nonlinear temperature rise (NTR) for $\alpha_T > 1$.

By imposing the thermal influence on the formulation, the force and moment resultants can be evaluated by the integration of Equation (46), which yields:

$$\begin{Bmatrix} \bar{N}^{th}(x) \\ \bar{M}_c^{th}(x) \\ \bar{M}_{nc}^{th}(x) \end{Bmatrix} = \Delta T \int_{-\frac{b}{2}}^{\frac{b}{2}} \int_{-\frac{h}{2}}^{\frac{h}{2}} \mathbb{E}^{th}(x, z_m, T) \alpha(x, z, T) \left(\frac{z_n}{h} + \frac{1}{2}\right)^{\alpha^T} \begin{Bmatrix} 1 \\ z_n \\ \mathrm{R}_n(z) \end{Bmatrix} dzdy \tag{47}$$

In the present work, the nonclassical equilibrium motion and the corresponding nonclassical boundary conditions of 2D-FG microbeams are obtained employing the Hamilton principle:

$$\int_{t_0}^{t_f} (\delta \mathbb{T} - \delta \mathbb{U} + \delta \mathbb{W}) = 0 \tag{48}$$

By substitution Equations (41)–(43) into Equation (48), the governing equations of the 2D-FG temperature-dependent thermomechanical microbeam under moving mass can be evaluated as:

$$\begin{aligned} u: \; & -\mathrm{I}_A(x) \frac{\partial^2 u}{\partial t^2} + \mathrm{I}_B(x) \frac{\partial^3 w}{\partial x \partial t^2} - \mathrm{I}_E(x) \frac{\partial^2 \phi}{\partial t^2} + \mathcal{A}_{11}(x) \frac{\partial^2 u}{\partial x^2} - \mathcal{B}_{11}(x) \frac{\partial^3 w}{\partial x^3} + \mathcal{E}_{11}(x) \frac{\partial^2 \phi}{\partial x^2} + \frac{\partial \mathcal{A}_{11}(x)}{\partial x} \frac{\partial u}{\partial x} \\ & - \frac{\partial \mathcal{B}_{11}(x)}{\partial x} \frac{\partial^2 w}{\partial x^2} + \frac{\partial \mathcal{E}_{11}(x)}{\partial x} \frac{\partial \phi}{\partial x} + f_u - \frac{\partial N}{\partial x} = 0 \end{aligned} \tag{49}$$

$$
\begin{aligned}
w:\ &\left\{-\mathrm{I}_B(x)\frac{\partial^3 u}{\partial x\partial t^2}-\frac{\partial \mathrm{I}_B(x)}{\partial x}\frac{\partial^2 u}{\partial t^2}+\mathrm{I}_D(x)\frac{\partial^4 w}{\partial x^2\partial t^2}+\frac{\partial \mathrm{I}_D(x)}{\partial x}\frac{\partial^3 w}{\partial x\partial t^2}-\mathrm{I}_A(x)\frac{\partial^2 w}{\partial t^2}-\mathrm{I}_F(x)\frac{\partial^3 \phi}{\partial x\partial t^2}-\frac{\partial \mathrm{I}_F(x)}{\partial x}\frac{\partial^2 \phi}{\partial t^2}\right\}\\
&+\left\{\mathcal{B}_{11}(x)\ \frac{\partial^3 u}{\partial x^3}+2\frac{\partial \mathcal{B}_{11}(x)}{\partial x}\ \frac{\partial^2 u}{\partial x^2}+\frac{\partial^2 \mathcal{B}_{11}(x)}{\partial x^2}\ \frac{\partial u}{\partial x}\right\}\\
&+\left\{-\mathcal{D}_{11}(x)\ \frac{\partial^4 w}{\partial x^4}-2\frac{\partial \mathcal{D}_{11}(x)}{\partial x}\ \frac{\partial^3 w}{\partial x^3}+\left\{-\frac{\partial^2 \mathcal{D}_{11}(x)}{\partial x^2}-\bar{N}^{th}(x)\right\}\ \frac{\partial^2 w}{\partial x^2}\right\}\\
&+\left\{\mathcal{F}_{11}(x)\frac{\partial^3 \phi}{\partial x^3}+2\frac{\partial \mathcal{F}_{11}(x)}{\partial x}\frac{\partial^2 \phi}{\partial x^2}+\frac{\partial^2 \mathcal{F}_{11}(x)}{\partial x^2}\frac{\partial \phi}{\partial x}\right\}\\
&+\left\{\mathcal{A}_{11}(x)\frac{\partial^2 u}{\partial x^2}+\frac{\partial \mathcal{A}_{11}(x)}{\partial x}\frac{\partial u}{\partial x}+\frac{1}{2}\frac{\partial B_{11}(x)}{\partial x}\frac{\partial^2 w}{\partial x^2}+\frac{1}{2}\frac{\partial^2 B_{11}(x)}{\partial x^2}\frac{\partial w}{\partial x}+\mathcal{E}_{11}(x)\frac{\partial^2 \phi}{\partial x^2}\right.\\
&\left.+\frac{\partial \mathcal{E}_{11}(x)}{\partial x}\frac{\partial \phi}{\partial x}\right\}-\frac{\partial^2 \bar{M}_c^{th}(x)}{\partial x^2}+\left\{P(x)\delta(x-vt)+q+\frac{\partial}{\partial x}\left(f_c-\frac{1}{2}f_c a_c(x)\right)\right\}=0
\end{aligned}
\tag{50}
$$

$$
\begin{aligned}
\phi:&\left\{-\mathrm{I}_E(x)\frac{\partial^2 u}{\partial t^2}+\mathrm{I}_F(x)\frac{\partial^3 w}{\partial x\partial t^2}-\mathrm{I}_H(x)\frac{\partial^2 \phi}{\partial t^2}\right\}+\left\{\mathcal{E}_{11}(x)\ \frac{\partial^2 u}{\partial x^2}+\frac{\partial \mathcal{E}_{11}(x)}{\partial x}\ \frac{\partial u}{\partial x}\right\}\\
&+\left\{-\mathcal{F}_{11}(x)\ \frac{\partial^3 w}{\partial x^3}-\frac{\partial \mathcal{F}_{11}(x)}{\partial x}\ \frac{\partial^2 w}{\partial x^2}\right\}+\left\{\mathcal{H}_{11}(x)\frac{\partial^2 \phi}{\partial x^2}+\frac{\partial \mathcal{H}_{11}(x)}{\partial x}\frac{\partial \phi}{\partial x}-\mathcal{B}_{xz}(x)\phi(x)\right\}\\
&-\left\{\frac{\partial \bar{M}_{nc}^{th}(x)}{\partial x}-\frac{1}{2}f_c a_c(x)\right\}=0
\end{aligned}
\tag{51}
$$

with the following boundary conditions:

$$
\boldsymbol{\delta u}\text{: }\mathbf{Either}\ \ u=\tilde{u}\ \ \mathbf{or}\ \ \mathcal{A}_{11}(x)\frac{\partial u}{\partial x}-\mathcal{B}_{11}(x)\ \frac{\partial^2 w}{\partial x^2}+\mathcal{E}_{11}(x)\frac{\partial \phi}{\partial x}-\bar{N}=0 \tag{52}
$$

$$
\begin{aligned}
\boldsymbol{\delta w}\text{: }\mathbf{Either}\ \ w=\tilde{w}\ \ \mathbf{or}\ \ &\left\{-\mathrm{I}_B(x)\frac{\partial^2 u}{\partial t^2}+\mathrm{I}_D(x)\frac{\partial^3 w}{\partial x\partial t^2}-\mathrm{I}_F(x)\frac{\partial^2 \phi}{\partial t^2}\right\}+\left\{\mathcal{B}_{11}(x)\ \frac{\partial^2 u}{\partial x^2}+\frac{\partial \mathcal{B}_{11}(x)}{\partial x}\ \frac{\partial u}{\partial x}\right\}\\
&+\left\{-\mathcal{D}_{11}(x)\ \frac{\partial^3 w}{\partial x^3}-\frac{\partial \mathcal{D}_{11}(x)}{\partial x}\ \frac{\partial^2 w}{\partial x^2}-N\frac{\partial w}{\partial x}\right\}+\left\{\mathcal{F}_{11}(x)\frac{\partial^2 \phi}{\partial x^2}+\frac{\partial \mathcal{F}_{11}(x)}{\partial x}\frac{\partial \phi}{\partial x}\right\}\\
&+\left\{\bar{V}-\left(f_c-\frac{1}{2}f_c a_c(x)\right)\right\}=0
\end{aligned}
\tag{53}
$$

$$
\boldsymbol{\delta\phi}\text{: }\mathbf{Either}\ \ \phi=\tilde{\phi}\ \ \mathbf{or}\ \ \mathcal{E}_{11}(x)\frac{\partial u}{\partial x}-\mathcal{F}_{11}(x)\ \frac{\partial^2 w}{\partial x^2}+\mathcal{H}_{11}(x)\ \frac{\partial \phi}{\partial x}-\bar{M}_c=0 \tag{54}
$$

$$
\frac{\boldsymbol{\partial\delta w}}{\boldsymbol{\partial x}}\text{: }\mathbf{Either}\ \ \frac{\partial w}{\partial x}=\frac{\overline{\partial w}}{\partial x}\ \ \mathbf{or}\ \ \mathcal{B}_{11}(x)\frac{\partial u}{\partial x}-\mathcal{D}_{11}(x)\ \frac{\partial^2 w}{\partial x^2}+\mathcal{F}_{11}(x)\frac{\partial \phi}{\partial x}+\{\bar{M}_c+\bar{M}_{nc}\}=0 \tag{55}
$$

## 4. Analytical Solution

To solve the system of partial differential equations of the SBDFG microbeam excited by a moving load, Equations (49)–(51), Galerkin's decomposition is adopted to reduce this set of equations into a system of ordinary differential equations. In this regard, the dynamic axial, transverse deflection, and the rotation of the SBDFG microbeam are truncated into n-modes as $w(x,t)=\sum_{n=1}^{\infty}W_n(t)\theta_w(x)$, $u(x,t)=\sum_{n=1}^{\infty}U_n(t)\theta_u(x)$, and $\phi(x,t)=\sum_{n=1}^{\infty}\Phi_n(t)\theta_\phi(x)$, in which the $\theta_w, \theta_u$, and $\theta_\phi$ denote the appropriate $n$th mode shapes of the SBDFG beam that satisfies the boundary conditions. $W_n(t)$ is deflection time-dependent for n$^{th}$ mode shapes. In the case of SS boundary conditions, the mode shapes are $\theta_w(x)=\sin(\alpha_n x)$ and $\theta_u(x)=\theta_\phi(x)=\cos(\alpha_n x)$ and $\alpha_n=n\pi/L$. For simplicity, a single-mode Galerkin decomposition is used, $\alpha_n=\alpha=\pi/L$.

Multiplying Equations (49)–(51) by $\cos(\alpha x)$ and $\sin(\alpha x)$, we can integrate the obtained equations with respect to $x$ from 0 to $L$.

By using the general property of the Dirac delta function and its Fourier series as $\delta(x,t)=\sum_{n=1}^{\infty}\sin(\alpha_n x)\sin(\alpha_n v_0 t)$, the following set of ODEs is obtained:

$$a_1\ddot{U}_n(t) + a_2U_n(t) + a_3\ddot{W}_n(t) + a_4W_n(t) + a_5\ddot{\Phi}_n(t) + a_6\Phi_n(t) = 0 \tag{56}$$

$$b_1\ddot{U}_n(t) + b_2U_n(t) + b_3\ddot{W}_n(t) + b_4W_n(t) + b_5\ddot{\Phi}_n(t) + b_6\Phi_n(t) = F_1\sin(\alpha_n v_0 t) \tag{57}$$

$$c_1\ddot{U}_n(t) + c_2U_n(t) + c_3\ddot{W}_n(t) + c_4W_n(t) + c_5\ddot{\Phi}_n(t) + c_6\Phi_n(t) = 0 \tag{58}$$

where the coefficients $a_i, b_i$, and $c_i$ are defined as $(i = 1, 2, \ldots 6)$

$$\begin{Bmatrix} a_1 & a_2 \\ a_3 & a_4 \\ a_5 & a_6 \end{Bmatrix} = \int_0^L \begin{Bmatrix} -\mathrm{I}_A(x)\theta_u & \mathcal{A}_{11}(x)\theta_u'' + \dfrac{\partial \mathcal{A}_{11}(x)}{\partial x}\theta_u' \\ \mathrm{I}_B(x)\theta_w' & -\mathcal{B}_{11}(x)\theta_w''' - \dfrac{\partial \mathcal{B}_{11}(x)}{\partial x}\theta_w'' \\ -\mathrm{I}_E(x)\theta_\phi & \mathcal{E}_{11}(x)\theta_\phi'' + \dfrac{\partial \mathcal{E}_{11}(x)}{\partial x}\theta_\phi' \end{Bmatrix} \cos(\alpha_m x)\, dx \tag{59}$$

$$\begin{Bmatrix} b_1 & b_2 \\ b_3 & b_4 \\ b_5 & b_6 \end{Bmatrix} = \int_0^L \begin{Bmatrix} -\mathrm{I}_B(x)\theta_u' - \dfrac{\partial \mathrm{I}_B(x)}{\partial x}\theta_u & \mathcal{B}_{11}(x)\theta_u''' + 2\dfrac{\partial \mathcal{B}_{11}(x)}{\partial x}\theta_u'' + \dfrac{\partial^2 \mathcal{B}_{11}(x)}{\partial x^2}\theta_u' \\ \mathrm{I}_D(x)\theta_w'' + \dfrac{\partial \mathrm{I}_D(x)}{\partial x}\theta_w' - \mathrm{I}_A(x)\theta_w & -\mathcal{D}_{11}(x)\theta_w'''' - 2\dfrac{\partial \mathcal{D}_{11}(x)}{\partial x}\theta_w''' + \left\{-\dfrac{\partial^2 \mathcal{D}_{11}(x)}{\partial x^2} - N_{th}\right\}\theta_w'' \\ -\mathrm{I}_F(x)\theta_\phi' - \dfrac{\partial \mathrm{I}_F(x)}{\partial x}\theta_\phi & \mathcal{F}_{11}(x)\theta_\phi''' + 2\dfrac{\partial \mathcal{F}_{11}(x)}{\partial x}\theta_\phi'' + \dfrac{\partial^2 \mathcal{F}_{11}(x)}{\partial x^2}\theta_\phi' \end{Bmatrix} \sin(\alpha_m x)\, dx \tag{60}$$

$$\begin{Bmatrix} c_1 & c_2 \\ c_3 & c_4 \\ c_5 & c_6 \end{Bmatrix} = \int_0^L \begin{Bmatrix} -\mathrm{I}_E(x)\theta_u & \mathcal{E}_{11}(x)\theta_u'' + \dfrac{\partial \mathcal{E}_{11}(x)}{\partial x}\theta_u' \\ \mathrm{I}_F(x)\theta_w' & -\mathcal{F}_{11}(x)\theta_w''' - \dfrac{\partial - \mathcal{F}_{11}(x)}{\partial x}\theta_w'' \\ -\mathrm{I}_H(x)\theta_\phi & \mathcal{H}_{11}(x)\theta_\phi'' + \dfrac{\partial \mathcal{H}_{11}(x)}{\partial x}\theta_\phi' - \mathcal{B}_{xz}(x)\theta_\phi \end{Bmatrix} \cos(\alpha_m x)\, dx \tag{61}$$

and $F_1 = -\int_0^L P(x)\sin(\alpha_n x)\sin(\alpha_m x)$

with the initial condition:

$$W_n(0) = \dot{W}_n(0) = U_n(0) = \dot{U}_n(0) = \Phi_n(0) = \dot{\Phi}_n(0) \tag{62}$$

To solve the system of equations in the time domain, Laplace transform (LT) is proposed with the following functions: $\mathcal{L}\{\ddot{W}_n(t)\} = s^2W_s(s) - sW_n(0) - \dot{W}_n(0)$, where $\mathcal{L}\{W_n(t)\} = W_s(s)$ and $\mathcal{L}\{\ddot{U}_n(t)\} = s^2U_s(s) - sU_n(0) - \dot{U}_n(0)$ and $\mathcal{L}\{\ddot{\Phi}_n(t)\} = s^2\Phi_s(s) - s\Phi_n(0) - \dot{\Phi}_n(0)$.

Finally, by using the initial conditions and applying Laplace transform (LT), the system of equations in Laplace form is obtained as follows:

$$(a_1s^2 + a_2)U_s + (a_3s^2 + a_4)W_s + (a_5s^2 + a_6)\Phi_s = 0 \tag{63}$$

$$(b_1s^2 + b_2)U_s + (b_3s^2 + b_4)W_s + (b_5s^2 + b_6)\Phi_s = \frac{F_1\alpha_n v_0}{(\alpha_n v_0)^2 + s^2} \tag{64}$$

$$(c_1s^2 + c_2)U_s + (c_3s^2 + c_4)W_s + (c_5s^2 + c_6)\Phi_s = 0 \tag{65}$$

Solving Equation (63)–(65), one derives:

$$W_s(s) = \frac{r_1s^4 + r_2s^2 + r_3}{\mathcal{K}_1s^6 + \mathcal{K}_2s^4 + \mathcal{K}_3s^2 + \mathcal{K}_4}\left(\frac{1}{(\alpha_n v_0)^2 + s^2}\right) \tag{66}$$

in which

$$\mathcal{K}_1 = a_1(b_3c_5 - b_5c_3) + a_3(b_5c_1 - b_1c_5) + a_5(b_1c_3 - b_3c_1) \tag{67}$$

$$\begin{aligned}\mathcal{K}_2 = {} & a_1(b_3c_6 + b_4c_5 - b_5c_4 - b_6c_3) + a_3(b_5c_2 + b_6c_1 - b_1c_6 - b_2c_5) + a_5(b_1c_4 + b_2c_3 - b_3c_2 - b_4c_1) \\ & + a_2(b_3c_5 - b_5c_3) + a_4(b_5c_1 - b_1c_5) + a_6(b_1c_3 - b_3c_1)\end{aligned} \tag{68}$$

$$\begin{aligned}\mathcal{K}_3 = {} & a_1(b_3c_6 + b_4c_5 - b_5c_4 - b_6c_3) + a_3(b_5c_2 + b_6c_1 - b_1c_6 - b_2c_5) + a_5(b_1c_4 + b_2c_3 - b_3c_2 - b_4c_1) \\ & + a_2(b_3c_5 - b_5c_3) + a_4(b_5c_1 - b_1c_5) + a_6(b_1c_3 - b_3c_1)\end{aligned} \tag{69}$$

$$\mathcal{K}_4 = \mathrm{a}_2(\mathrm{b}_4\mathrm{c}_6 - \mathrm{b}_6\mathrm{c}_4) + \mathrm{a}_4(\mathrm{b}_6\mathrm{c}_2 - \mathrm{b}_2\mathrm{c}_6) + \mathrm{a}_6(\mathrm{b}_2\mathrm{c}_4 - \mathrm{b}_4\mathrm{c}_2) \tag{70}$$

and

$$\begin{Bmatrix} r_1 \\ r_2 \\ r_3 \end{Bmatrix} = F_1\alpha_n v_0 \begin{Bmatrix} a_1c_5 - a_5c_1 \\ a_1c_6 + a_2c_5 - a_5c_2 - a_6c_1 \\ a_2c_6 - a_6c_2 \end{Bmatrix} \tag{71}$$

The roots of the sixth-order polynomial of the dominator of $W_s(s)$ can be found as

$$\begin{Bmatrix} \psi_{1,2} \\ \psi_{3,4} \\ \psi_{5,6} \end{Bmatrix} = \begin{Bmatrix} \pm\sqrt{\dfrac{\Delta_1 - (12\,\mathcal{K}_1\mathcal{K}_3 - 4\mathcal{K}_2^2) - 2\mathcal{K}_2\Delta_1}{6\mathcal{K}_1\,\Delta_1}} \\ \pm\sqrt{\dfrac{1}{12\mathcal{K}_1\,\Delta_1}\left[-\Delta_1^2 + (12\,\mathcal{K}_1\mathcal{K}_3 - 4\mathcal{K}_2^2) - 4\mathcal{K}_2\Delta_1 + \sqrt{3}i(\Delta_1^2 + 12\mathcal{K}_1\mathcal{K}_3 - 4\mathcal{K}_2^2)\right]} \\ \pm\sqrt{\dfrac{1}{12\mathcal{K}_1\,\Delta_1}\left[-\Delta_1^2 + (12\,\mathcal{K}_1\mathcal{K}_3 - 4\mathcal{K}_2^2) - 4\mathcal{K}_2\Delta_1 - \sqrt{3}i(\Delta_1^2 + 12\mathcal{K}_1\mathcal{K}_3 - 4\mathcal{K}_2^2)\right]} \end{Bmatrix} \tag{72}$$

where

$$\Delta_1 = \sqrt[3]{-108\,\mathcal{K}_4\,\mathcal{K}_1^2 + 36\,\mathcal{K}_3\,\mathcal{K}_2\,\mathcal{K}_1 + 12\sqrt{3}\,\mathcal{K}_1\sqrt{27\,\mathcal{K}_4^2\mathcal{K}_1^2 - 18\,\mathcal{K}_4\,\mathcal{K}_1\,\mathcal{K}_2\,\mathcal{K}_3 + 4\,\mathcal{K}_4\mathcal{K}_2^3 + 4\,\mathcal{K}_1\mathcal{K}_3^3 - \mathcal{K}_2^2\mathcal{K}_3^2} - 8\,\mathcal{K}_2^3} \tag{73}$$

By using the inverse Laplace transform (ILT) to $W_s(s)$, the dynamic response can be obtained by

$$w(x,t) = \frac{1}{\mathcal{K}_1 d_0}(d_1\sinh(\psi_5 t) + d_2\sinh(\psi_1 t) - d_3\sinh(\psi_3 t) + d_4\sin(\alpha_n v_0 t))\sin(\alpha_n x) \tag{74}$$

in which

$$\begin{Bmatrix} d_0 \\ d_1 \\ d_2 \\ d_3 \\ d_4 \end{Bmatrix} = \begin{Bmatrix} \psi_1\psi_3\psi_5\alpha_n v_0\,(\psi_1^2 - \psi_3^2)(\psi_1^2 - \psi_5^2)(\psi_3^2 - \psi_5^2)((\alpha_n v_0)^2 + \psi_5^2)((\alpha_n v_0)^2 + \psi_3^2)((\alpha_n v_0)^2 + \psi_1^2) \\ \alpha_n v_0\,\psi_3\psi_1(\psi_1^2 - \psi_3^2)((\alpha_n v_0)^2 + \psi_1^2)((\alpha_n v_0)^2 + \psi_3^2)(\psi_5^4 r_1 + \psi_5^2 r_2 + r_3) \\ \alpha_n v_0\,\psi_3\psi_5(\psi_3^2 - \psi_5^2)((\alpha_n v_0)^2 + \psi_3^2)((\alpha_n v_0)^2 + \psi_5^2)(\psi_1^4 r_1 + \psi_1^2 r_2 + r_3) \\ \alpha_n v_0\psi_1\psi_5(\psi_1^2 - \psi_5^2)\,((\alpha_n v_0)^2 + \psi_5^2)((\alpha_n v_0)^2 + \psi_1^2)(\psi_3^4 r_1 + \psi_3^2 r_2 + r_3) \\ \psi_1\psi_3\psi_5(\psi_1^2 - \psi_5^2)(\psi_3^2 - \psi_5^2)(\psi_1^2 - \psi_3^2)(-(\alpha_n v_0)^4 r_1 + (\alpha_n v_0)^2 r_2 - r_3) \end{Bmatrix} \tag{75}$$

The following nondimensional quantities are proposed in the analysis to generalize the problem:

$$\bar{w}(x,t) = \frac{w(x,t)}{D_0}, \qquad \bar{\omega}_1 = \omega_1 L^2\sqrt{\rho_c bh/E_c I}\,, \qquad \bar{v} = \frac{v}{V_c}, \qquad V_c = \frac{L\omega_1}{\pi}, \qquad \tau = \frac{t}{L/v} \tag{76}$$

where $\bar{w}(x,t)$ represents the normalized dynamic deflections. $D_0$ is the peak transverse deflection of the beam with full metal constituent under a point load $P_0$ ($D_0 = P_0\,L^3/48E_m\,I$), $I = bh^3/12$. $\omega_1$ is the dimensionless first natural frequency. $\bar{v}$ is the dimensionless velocity of the moving load. $V_c$ is the critical velocity (the maximum magnitudes of the maximum deflections to occur). τ ($0 < \tau < 1$) signifies the dimensionless time. When $\tau > 1$, the load is away from the beam.

## 5. Model Validation

This section presents the convergence and accuracy of the present model and solution procedure by comparing our results with previous works. Since there is no previous work considering bidirectional sigmoidal graded beams, the SBDFG is validated with power law results for the $k_z = 1$ case and also for the homogeneous case $k_z = k_x = 0$. Table 1 compares the peak deflections $(\bar{w}_p)$ and the corresponding absolute velocities $(v_p)$ of an SS transverse power functionally graded (TPFG) SUS304/Al2O3 beam with the results reported by [29,35,69,70] at $\Omega_f = 0$ (ignoring temperature effect). In Table 1, the beam is composed of a mixture of metal SUS304 stainless steel ($E_m$ = 210 GPa and mass density of $\rho_m^B$ = 7800 kg/m$^3$) and ceramic ($Al_2O_3$) ($E_c$ = 390 GPa, and $\rho_c^B$ = 3960 kg/m$^3$). The beam has 0.4 m width, 0.9 m thickness, and 20 m length. As concluded, the current results for dynamic deflection and absolute velocity are close to all previous works, within 1% maximum deviation.

**Table 1.** Peak normalized dynamic deflection $\bar{w}_p$ and corresponding absolute velocity $v_p$ of simply supported beams, at $T(z) = 0$.

| | Source | Pure SUS304 | $k_z$ = 1.0 | Pure $Al_2O_3$ |
|---|---|---|---|---|
| $\bar{w}_p$ | Present, SBDFG | 1.7475 | 1.2641 | 0.9433 |
| | Ref. [29] (RBT) | 1.7384 | 1.2575 | 0.9384 |
| | Ref. [70] (TBT) | 1.7379 | 1.2287 | 0.9382 |
| | Ref. [69] (TBT) | 1.7420 | 1.2566 | 0.9380 |
| | Ref. [35] (EBT) | 1.7324 | 1.2503 | 0.9328 |
| $v_p$ | Present, SBDFG | 130 | 177 | 249 |
| | Ref. [29] (RBT) | 131 | 178 | 252 |
| | Ref. [70] (TBT) | 132 | 179 | 252 |
| | Ref. [69] (TBT) | 131 | 178 | 251 |
| | Ref. [35] (EBT) | 132 | 179 | 252 |

To validate the temperature effect, a beam with constituents of metal (SUS304 stainless steel) and silicon nitride ($Si_3N_4$) is considered. The material properties are temperature-dependent according to Equation (3) for SUS304 and $Si_3N_4$. The constants $\mathcal{P}_0, \mathcal{P}_{-1}, \mathcal{P}_1, \mathcal{P}_2$, and $\mathcal{P}_3$ are given in Table 2 for metal and ceramic phases. Considering the validation of the temperature effect, the fundamental dimensionless frequency $\bar{\omega}$ of the simply supported TSFG SUS304/$Si_3N_4$ beam is validated by Ebrahimi and Salari [71] for EBT at different temperature differences ΔT (LTR), as in Table 3. As seen, the natural frequencies of isotropic and FG material are decreased with increasing temperature differences or by increasing the gradation index through thickness. The same observation was predicted by Ebrahimi and Salari [71].

**Table 2.** Temperature-dependent coefficients for metal (SUS304) and ceramic ($Si_3N_4$) constituents [71].

| Material | Properties | $\mathcal{P}_{-1}$ | $\mathcal{P}_0$ | $\mathcal{P}_1$ | $\mathcal{P}_2$ | $\mathcal{P}_3$ |
|---|---|---|---|---|---|---|
| SUS304 (Metal) | $E$(Pa) | 0 | $201.04 \times 10^9$ | $3.079 \times 10^{-4}$ | $-6.534 \times 10^{-7}$ | 0 |
| | $\rho$(Kg/m$^3$) | 0 | 8166 | 0 | 0 | 0 |
| | $\nu$ | 0 | 0.3262 | 0 | 0 | 0 |
| | $\alpha$(1/K) | 0 | $12.330 \times 10^{-6}$ | $8.086 \times 10^{-4}$ | 0 | 0 |
| $Si_3N_4$ (Ceramic) | $E$(Pa) | 0 | $348.43 \times 10^9$ | $-3.070 \times 10^{-4}$ | $2.160 \times 10^{-7}$ | $-8.946 \times 10^{-11}$ |
| | $\rho$(Kg/m$^3$) | 0 | 2170 | 0 | 0 | 0 |
| | $\nu$ | 0 | 0.24 | 0 | 0 | 0 |
| | $\alpha$(1/K) | 0 | $5.8723 \times 10^{-6}$ | $9.095 \times 10^{-4}$ | 0 | 0 |

**Table 3.** Comparison of the fundamental dimensionless frequency $\bar{\omega}$ of simply supported TFG SUS304/$Si_3N_4$ beams at different temperature differences $\Delta T(LTR)$.

| Source | $\Delta T$ | $k_z$ = 0.0 | $k_z$ = 1.0 |
|---|---|---|---|
| Present, SBDFG | 10 | 9.7643 | 5.7294 |
| Ref. [71] (TBT) | | 9.6461 | 5.7717 |
| Present, SBDFG | 30 | 9.6074 | 5.5964 |
| Ref. [71] (TBT) | | 9.4538 | 5.6105 |
| Present, SBDFG | 60 | 9.3682 | 5.3889 |
| Ref. [71] (TBT) | | 9.1475 | 5.3537 |

In Figures 2 and 3, the fundamental frequency and the maximum dynamic response at the center are calculated to give comparisons with two available results in the literature. First, a comparison is performed with Liu et al. [41], showing the dependency of the dimensionless fundamental frequency of the SBDFG on temperature under LTR. Secondly, to show the accuracy of the present analytical solution, the relation between dimensionless dynamic deflection and moving load speed is validated by Abdelrahman et al. [44] and Şimşek [36]. Through these validations and as can be observed, there is good agreement with the literature results, which demonstrates the validity of the present model and its analytical solution.

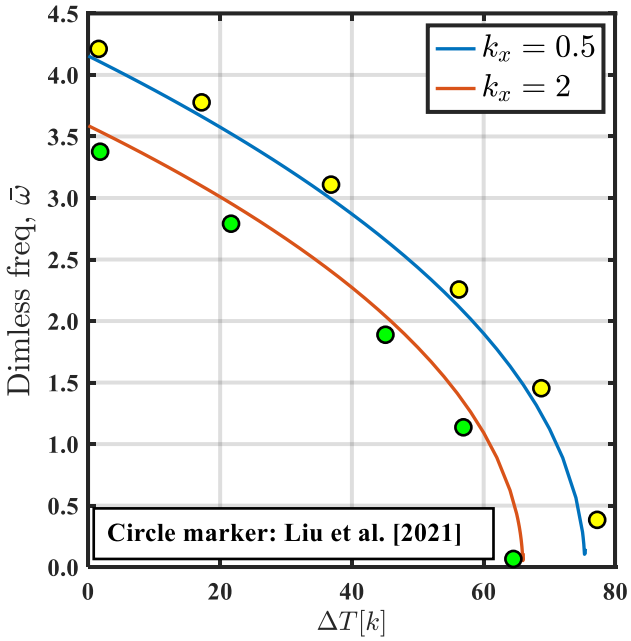


**Figure 2.** Comparison of the dependency of the dimensionless fundamental frequency of the beam at different temperature differences $\Delta T$ under LTR for $k_x = (0.5, 2), k_z = 0.5, lcs = 0.25\ h$.

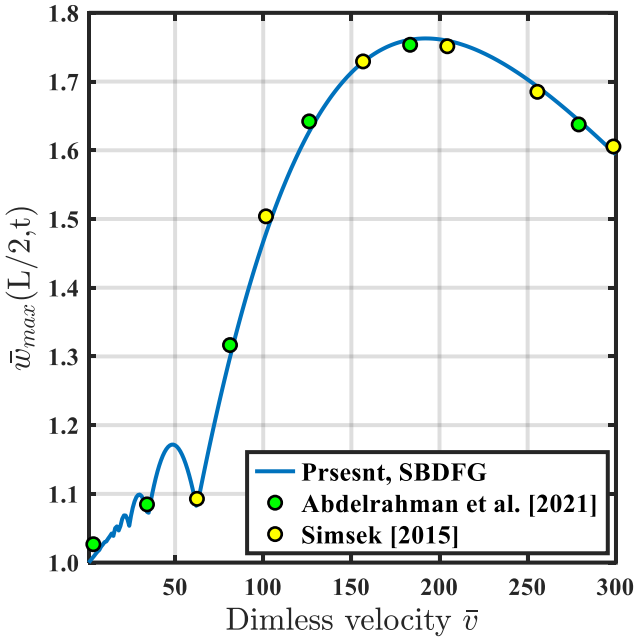


**Figure 3.** The variation in the dynamic deflection at the center of the beam vs. moving load velocity.

## 6. Numerical Results

In this section, the influences of different key parameters on the dynamical response of SBDFG microbeams under a moving harmonic load are extensively explored, i.e., the transverse and axial gradient indices, velocity, frequency, temperature, and the small-scale effects due to the microstructure energy. Consider a simply supported SBDFG microbeam made of metal (SUS304) and ceramic ($Si_3N_4$) with the material properties in Table 2. In the following results, the material length scale constants $\mathcal{P}_0$ for metal and ceramic phases are $l_m = l_c = l = 22.5$ μm, and the other material length constants are set to zero [65,72]. The beam dimensions are $h = b = 2l$ and $L = 25h$. The other geometrical and material parameters are fixed through analysis.

### *6.1. Influence of the Gradation Indices*

Variations in the dimensionless fundamental frequency of SBDFG microbeams with SS boundaries vs. temperature variations are portrayed in Figures 4 and 5, respectively. From Figures 4 and 5, we can conclude that frequencies of SBDFG microbeams reduce with the rise in temperature until reaching the critical frequency temperature. This is because the geometrical stiffness decreases when the temperature rises without any variation in equivalent mass. The frequency reaches zero at the critical temperature point. After that, the stiffness induced by thermal load is higher than the structural stiffness; hence, the increase in temperature yields higher frequency after the branching point [71]. The branching point of the SBDFG microbeam is delayed by consideration of the lower axial gradient index, as seen in Figure 5. However, by increasing the transverse gradation index of the SBDFG microbeam, the critical temperature will be increased insignificantly, as concluded from Figure 4.

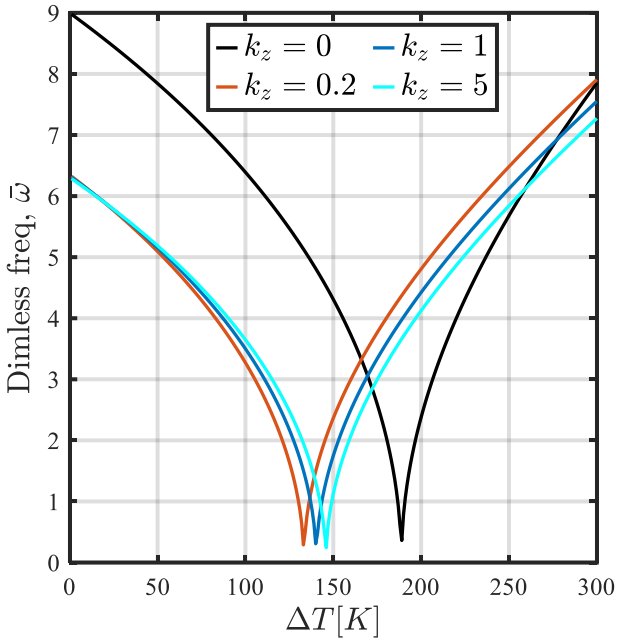


**Figure 4.** Influence of the transverse gradient index on the dimensionless fundamental frequency at different temperature differences $\Delta T$ under LTR and based on classical analysis $(l = 0, k_x = 0.2)$.

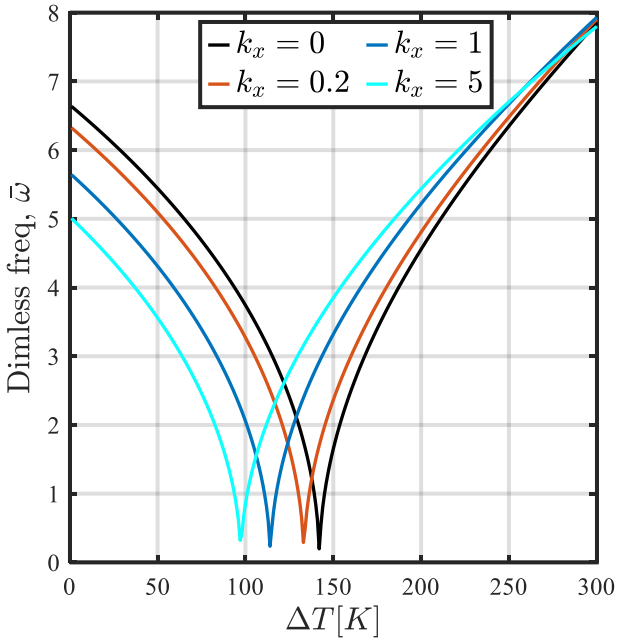


**Figure 5.** Influence of the axial gradient index on the dimensionless fundamental frequency at different temperature differences $\Delta T$ under LTR and based on classical analysis $(l = 0, k_z = 0.2)$.

Figures 6 and 7 illustrate the variation in the maximum normalized central dynamic deflection (dynamic magnification factor, $\bar{w}_{max}(L/2, t)$) vs. the dimensionless moving velocity at different values of $k_z$ and $k_x$, respectively. Both temperature-dependent and -independent LTR are considered at $\Delta T$ = 80. It is depicted from Figures 6 and 7 that $\bar{w}_{max}(L/2, t)$, over the entire time history, both increases and decreases, then increases to reach the peak value when the velocity reaches critical values. After that, $\bar{w}_{max}$ gradually decreases as the moving load velocity increases, which is consistent with Olsson's observation [73]. The velocity at which $\bar{w}_{max}$ attains its peak value is denoted as the beam critical velocity [74]. At lower velocities of the moving load, the repeated increase and decrease in the $\bar{w}_{max}$ is due to the beam oscillations. It is noted that by increasing the

gradation index through the thickness, the dynamic deflection increases for temperature-independent material. However, in the case of temperature-dependent material, increasing in $k_z$ from 0 to 0.2, the dynamic deflection increases significantly, and after that, dynamic deflection reduces by increasing the gradation index $k_z$. The effect of gradation index in the axial direction on the dynamic deflection is increased significantly in the case of LTR relative to temperature-independent material, as seen from Figure 7. The maximum deflection increased from 2.1 to 6.1 as $k_x$ changed from 0 to 5 in the case of LTR. However, it increased from 0.9 to 1.2 as $k_x$ changed from 0 to 5 in the case of temperature-independent material.

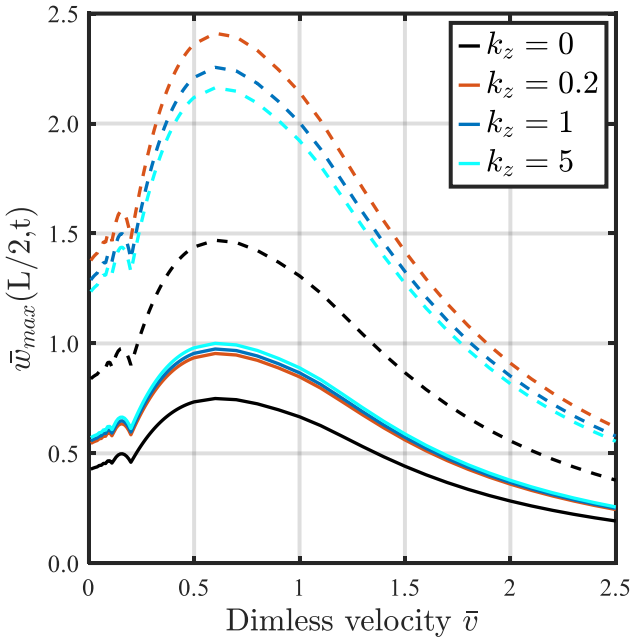


**Figure 6.** Influence of the transverse gradient index on the variation in the maximum normalized central dynamic deflection with the velocity ($k_x = 0.2$); (–) temperature-independent, (- -) temperature-dependent ($\Delta T = 80, LTR$).

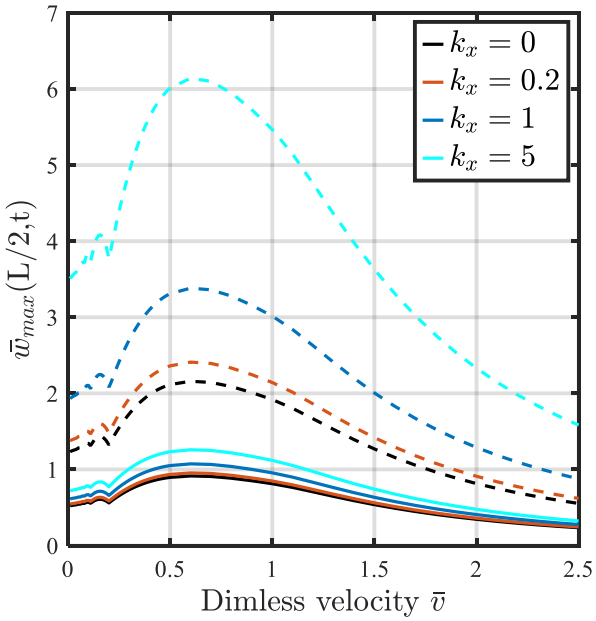


**Figure 7.** Influence of the axial gradient index on the variation in the maximum normalized central dynamic deflection with the velocity ($k_z = 0.2$); (__) temperature-independent, (- -) temperature-dependent ($\Delta T = 80, LTR$).

*6.2. Influence of Temperature Distribution*

The impact of temperature distribution type on the dynamic deflection of the SBDFG microbeam is described in this subsection. The temperature rise for linear temperature rise (LTR) and nonlinear temperature rise (NTR) distribution is assumed as $\Delta T = 100\,[K]$ *by* adjusting the initial temperature $T_0$ to room temperature at 300 K. Figure 8 shows that different temperature formulations and the moving velocity considerably affect the amplitude of dynamic deflection. Obviously, the temperature for the LTR type is larger than that for both the NTR type and temperature-independent material. As seen, by increasing the velocity, the profile of dynamic deflection vs. time $\tau$ is changed completely from oscillatory to parabolic to exponential functions. Thus, it can be concluded that the dynamic deflection profile response is dependent on the velocity of the moving mass.

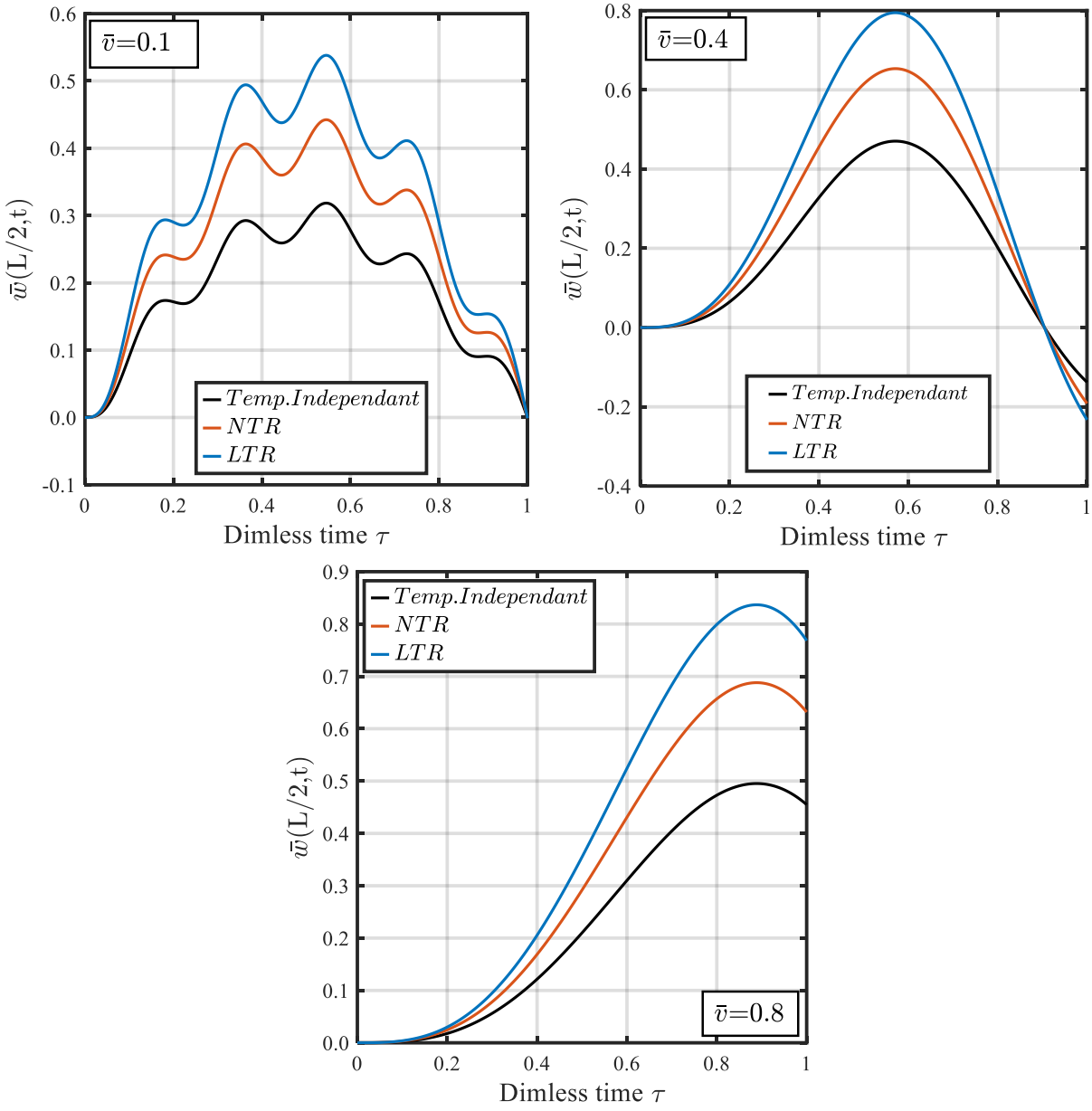


**Figure 8.** Influence of temperature distribution (temperature-independent, LTR and NTR with $\alpha_T$ = 2) on the dimensionless central deflection vs. time under a uniform moving load ($k_x$ = $k_z$ = 0.2) at $\bar{v}$ = 0.1, 0.4, and 0.8 and $\Delta T$ = 100.

*6.3. Influence of the Moving Load Velocity*

Figure 9 shows that for both classical (CL) and couple stress (CS) formulations, the moving velocity considerably affects the amplitude of dynamic deflection. The shapes of the time history curves are strongly affected by the moving velocity. The number of vibration cycles of the microbeam is enlarged at low velocities of the moving load because the ratio of moving load velocity to critical velocity becomes low.

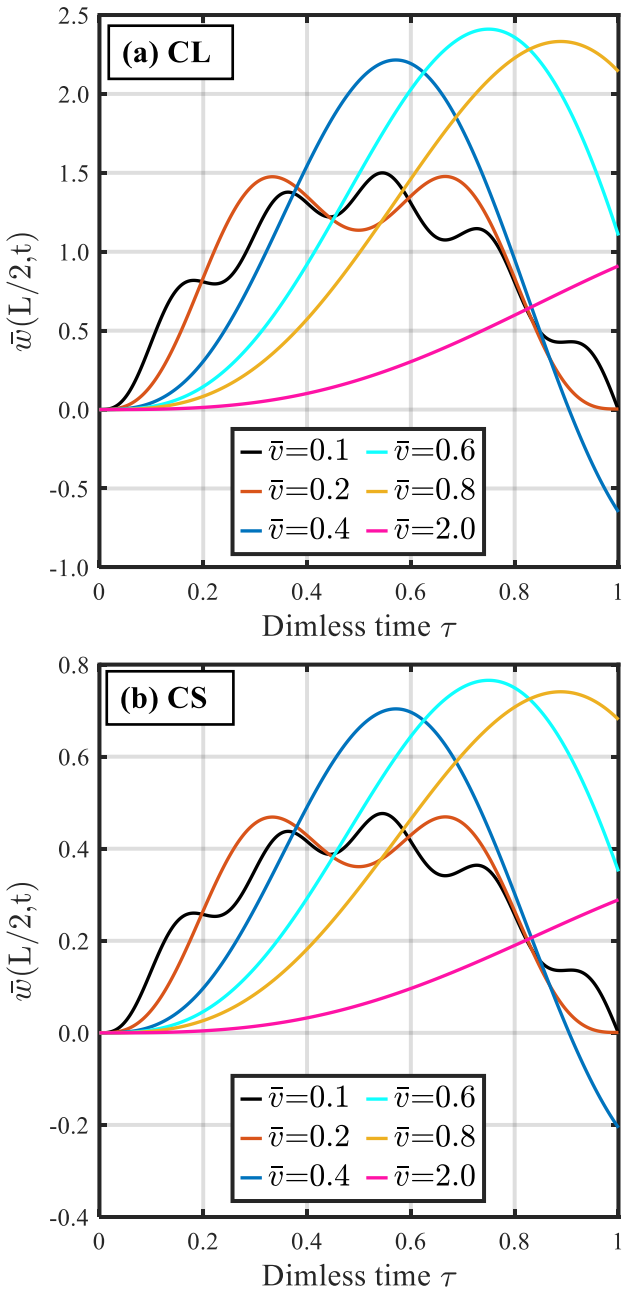


**Figure 9.** Influence of the dimensionless velocity on the variation in the dimensionless central deflection vs. the dimensionless time under a uniform moving load based on CL and CS formulations ($\Delta T = 80, LTR, k_x = k_z = 0.2$).

## 7. Conclusions

A dynamic response in closed-form solutions for sigmoid bidirectional functionally graded microbeams excited by a moving harmonic mechanical load under a thermal environment was developed by considering the microstructure effect. Temperature-

dependent thermomechanical materials with linear and nonlinear temperature profiles were considered. The nonclassical equations of motion and boundary conditions were developed and solved by Galerkin's decomposition technique in conjunction with Laplace transform and the implicit Newmark time integration method. The main points can be drawn from this analysis as follows:

- ✓ Fundamental frequencies of SBDFG microbeams reduce with a rise in temperature until it reaches the critical frequency temperature. This is because the geometrical stiffness decreases when the temperature rises without any variation in equivalent mass.
- ✓ By increasing the gradation index through the thickness, the dynamic deflection increases for temperature-independent material. However, in the case of temperature-dependent material, increasing in $k_z$ from 0 to 0.2, the dynamic deflection increased significantly, and after that, dynamic deflection reduced with the increasing gradation index $k_z$.
- ✓ The effect of gradation index in the axial direction on the dynamic deflection is increased significantly in the case of LTR relative to temperature-independent material.
- ✓ The temperature for the LTR type is larger than that for both the NTR type and temperature-independent material. As seen, by increasing the velocity, the profile of dynamic deflection vs. time $\tau$ is changed completely from oscillatory to parabolic to exponential functions. Therefore, the dynamic deflection profile response is dependent on the velocity of the moving mass.
- ✓ The shapes of the time history curves are strongly affected by the moving velocity. The number of vibration cycles of the microbeam is enlarged at low velocities of the moving load because the ratio of moving load velocity to critical velocity becomes low.

**Author Contributions**: Conceptualization, M.A.A., M.A.E.; Methodology, M.A.A.; Software, M.A.A., R.A.S.; Validation, R.A.S., A.M.; Formal analysis, M.A.A., R.A.S., A.M.; Investigation, M.A.E., A.M.; Resources, A.M. and M.A.E.; Data curation, R.A.S., M.A.A.; Writing—original draft, M.A.A., R.A.S.; Writing——review & editing, A.M., M.A.E.; Funding acquisition, A.M. All authors have read and agreed to the published version of the manuscript.

**Funding:** This research was funded by the Institutional Fund Projects under grant no. IFPIP (1677-135-1443).

**Informed Consent Statement:** Not applicable.

**Data Availability Statement:** Not applicable.

**Acknowledgments:** This research was funded by the Institutional Fund Projects under grant no. IFPIP (1677-135-1443). The authors gratefully acknowledge technical and financial support provided by the Ministry of Education and King Abdulaziz University, DSR in Jeddah, Saudi Arabia.

**Conflicts of Interest:** The authors declare no conflicts of interest.

## References

1. Attia, M.A.; Shanab, R.A. Vibration characteristics of two-dimensional FGM nanobeams with couple stress and surface energy under general boundary conditions. *Aerosp. Sci. Technol.* **2021**, *111*, 106552. https://doi.org/10.1016/j.ast.2021.106552.
2. Sayyad, A.S.; Ghugal, Y.M. Modeling and analysis of functionally graded sandwich beams: A review. *Mech. Adv. Mater. Struct.* **2019**, *26*, 1776–1795. https://doi.org/10.1080/15376494.2018.1447178.
3. Zhao, S.; Zhang, Y.; Wu, H.; Zhang, Y.; Yang, J. Functionally graded graphene origami-enabled auxetic metamaterial beams with tunable buckling and postbuckling resistance. *Eng. Struct.* **2022**, *268*, 114763. https://doi.org/10.1016/j.engstruct.2022.114763.
4. Xiao, S.; Cao, Y.; Wu, G.; Guo, Y.; Gao, G.; Chen, S.; Liu, P.; Wang, Z.; Li, P.; Yu, J.; et al. Influence of the distributed grounding layout for intercity trains on the 'train-rail' circumflux. *IEEE Trans. Circuits Syst. II Express Briefs* 2022, *early access*. https://doi.org/10.1109/TCSII.2022.3223984.
5. Melaibari, A.; Abdelrahman, A.A.; Hamed, M.A.; Abdalla, A.W.; Eltaher, M.A. Dynamic Analysis of a Piezoelectrically Layered Perforated Nonlocal Strain Gradient Nanobeam with Flexoelectricity. *Mathematics* **2022**, *10*, 2614. https://doi.org/10.3390/math10152614.

6. Ahmadi, I. Vibration analysis of 2D-functionally graded nanobeams using the nonlocal theory and meshless method. *Eng. Anal. Bound. Elem.* **2021**, *124*, 142–154. https://doi.org/10.1016/j.enganabound.2020.12.010.
7. Eltaher, M.A.; Mohamed, N. Nonlinear stability and vibration of imperfect CNTs by doublet mechanics. *Appl. Math. Comput.* **2020**, *382*, 125311. https://doi.org/10.1016/j.amc.2020.125311.
8. Asghari, M.; Rahaeifard, M.; Kahrobaiyan, M.H.; Ahmadian, M.T. The modified couple stress functionally graded Timoshenko beam formulation. *Mater. Des.* **2011**, *32*, 1435–1443. https://doi.org/10.1016/j.matdes.2010.08.046.
9. Şimşek, M. Buckling of Timoshenko beams composed of two-dimensional functionally graded material (2D-FGM) having different boundary conditions. *Compos. Struct.* **2016**, *149*, 304–314. https://doi.org/10.1016/j.compstruct.2016.04.034.
10. Nejad, M.Z.; Hadi, A. Non-local analysis of free vibration of bi-directional functionally graded Euler–Bernoulli nano-beams. *Int. J. Eng. Sci.* **2016**, *105*, 1–11. https://doi.org/10.1016/j.ijengsci.2016.04.011.
11. Nejad, M.Z.; Hadi, A.; Rastgoo, A. Buckling analysis of arbitrary two-directional functionally graded Euler–Bernoulli nano-beams based on nonlocal elasticity theory. *Int. J. Eng. Sci.* **2016**, *103*, 1–10. https://doi.org/10.1016/j.ijengsci.2016.03.00.
12. Mirafzal, A.; Fereidoon, A. Dynamic characteristics of temperature-dependent viscoelastic FG nanobeams subjected to 2D-magnetic field under periodic loading. *Appl. Phys. A* **2017**, *123*, 247. https://doi.org/10.1007/s00339-017-0829-1.
13. Shafiei, N.; Kazemi, M. Buckling analysis on the bi-dimensional functionally graded porous tapered nano-/micro-scale beams. *Aerosp. Sci. Technol.* **2017**, *66*, 1–11. https://doi.org/10.1016/j.ast.2017.02.019.
14. Shafiei, N.; Mirjavadi, S.S.; MohaselAfshari, B.; Rabby, S.; Kazemi, M. Vibration of two-dimensional imperfect functionally graded (2D-FG) porous nano-/micro-beams. *Comput. Methods Appl. Mech. Eng.* **2017**, *322*, 615–632. https://doi.org/10.1016/j.cma.2017.05.007.
15. Rajasekaran, S.; Khaniki, H.B. Free vibration analysis of bi-directional functionally graded single/multi-cracked beams. *Int. J. Mech. Sci.* **2018**, *144*, 341–356. https://doi.org/10.1016/j.ijmecsci.2018.06.004.
16. Sahmani, S.; Safaei, B. Nonlinear free vibrations of bi-directional functionally graded micro/nano-beams including nonlocal stress and microstructural strain gradient size effects. *Thin-Walled Struct.* **2019**, *140*, 342–356. https://doi.org/10.1016/j.tws.2019.03.045.
17. Sahmani, S.; Safaei, B. Nonlocal strain gradient nonlinear resonance of bi-directional functionally graded composite micro/nano-beams under periodic soft excitation. *Thin-Walled Struct.* **2019**, *143*, 106226. https://doi.org/10.1016/j.tws.2019.106226.
18. Tang, Y.; Ding, Q. Nonlinear vibration analysis of a bi-directional functionally graded beam under hygro-thermal loads. *Compos. Struct.* **2019**, *225*, 111076. https://doi.org/10.1016/j.compstruct.2019.111076.
19. Tang, Y.; Lv, X.; Yang, T. Bi-directional functionally graded beams: Asymmetric modes and nonlinear free vibration. *Compos. Part B Eng.* **2019**, *156*, 319–331. https://doi.org/10.1016/j.compositesb.2018.08.140.
20. Attia, M.A.; Mohamed, S.A. Thermal vibration characteristics of pre/post-buckled bi-directional functionally graded tapered microbeams based on modified couple stress Reddy beam theory. *Eng. Comput.* **2020**, *38*, 2079–2105. https://doi.org/10.1007/s00366-020-01188-4.
21. Barati, A.; Hadi, A.; Nejad, M.Z.; Noroozi, R. On vibration of bi-directional functionally graded nanobeams under magnetic field. *Mech. Based Des. Struct. Mach.* **2020**, *50*, 468–485. https://doi.org/10.1080/15397734.2020.1719507.
22. Ghatage, P.S.; Kar, V.R.; Sudhagar, P.E. On the numerical modelling and analysis of multi-directional functionally graded composite structures: A review. *Compos. Struct.* **2020**, *236*, 111837. https://doi.org/10.1016/j.compstruct.2019.111837.
23. Karami, B.; Janghorban, M.; Rabczuk, T. Dynamics of two-dimensional functionally graded tapered Timoshenko nanobeam in thermal environment using nonlocal strain gradient theory. *Compos. Part B Eng.* **2020**, *182*, 107622. https://doi.org/10.1016/j.compositesb.2019.107622.
24. Guo, L.; Zhao, S.; Guo, Y.; Yang, J.; Kitipornchai, S. Bandgaps in functionally graded phononic crystals containing graphene origami-enabled metamaterials. *Int. J. Mech. Sci.* **2022**, *240*, 107956. https://doi.org/10.1016/j.ijmecsci.2022.107956.
25. Zhao, S.; Zhang, Y.; Zhang, Y.; Zhang, W.; Yang, J.; Kitipornchai, S. Data-driven modeling for thermo-elastic properties of vacancy-defective graphene reinforced nanocomposites with its application to functionally graded beams. *Eng. Comput.* **2022**, 1–17. https://doi.org/10.1007/s00366-022-01710-w.
26. Daikh, A.A.; Houari MS, A.; Eltaher, M.A. A novel nonlocal strain gradient Quasi-3D bending analysis of sigmoid functionally graded sandwich nanoplates. *Compos. Struct.* **2021**, *262*, 113347. https://doi.org/10.1016/j.compstruct.2020.113347.
27. Daikh, A.A.; Houari MS, A.; Belarbi, M.O.; Chakraverty, S.; Eltaher, M.A. Analysis of axially temperature-dependent functionally graded carbon nanotube reinforced composite plates. *Eng. Comput.* **2021**, *38*, 2533–2554. https://doi.org/10.1007/s00366-021-01413-8.
28. Soni, S.K.; Thomas, B.; Swain, A.; Roy, T. Functionally graded carbon nanotubes reinforced composite structures: An extensive review. *Compos. Struct.* **2022,** *299*, 116075. https://doi.org/10.1016/j.compstruct.2022.116075.
29. Attia, M.A.; Shanab, R.A. On the dynamic response of bi-directional functionally graded nanobeams under moving harmonic load accounting for surface effect. *Acta Mech.* **2022**, *233*, 3291–3317. https://doi.org/10.1007/s00707-022-03243-1.
30. Zhao, S.; Zhao, Z.; Yang, Z.; Ke, L.; Kitipornchai, S.; Yang, J. Functionally graded graphene reinforced composite structures: A review. *Eng. Struct.* **2020**, *210*, 110339. https://doi.org/10.1016/j.engstruct.2020.110339.
31. Assie, A.E.; Mohamed, S.M.; Shanab, R.A.; Abo-bakr, R.M.; Eltaher, M.A. Static Buckling of 2D FG Porous Plates Resting on Elastic Foundation based on Unified Shear Theories. *J. Appl. Comput. Mech.* **2023**, *9*, 239–258. https://doi.org/10.22055/jacm.2022.41265.3723.

32. Eglin, M.; Eriksson, M.A.; Carpick, R.W. Microparticle manipulation using inertial forces. *Appl. Phys. Lett.* **2006**, *88*, 091913. https://doi.org/10.1063/1.2172401.
33. Roudbari, M.A.; Jorshari, T.D.; Arani, A.G.; Lü, C.; Rabczuk, T. Transient responses of two mutually interacting single-walled boron nitride nanotubes induced by a moving nanoparticle. *Eur. J. Mech.-A/Solids* **2020**, *82*, 103978. https://doi.org/10.1016/j.euromechsol.2020.103978.
34. Abdelrahman, A.A.; Ashry, M.; Alshorbagy, A.E.; Abdallah, W.S. On the mechanical behavior of two directional symmetrical functionally graded beams under moving load. *Int. J. Mech. Mater. Des.* **2021**, *17*, 563–586. https://doi.org/10.1007/s10999-021-09547-9.
35. Şimşek, M.; Kocatürk, T. Free and forced vibration of a functionally graded beam subjected to a concentrated moving harmonic load. *Compos. Struct.* **2009**, *90*, 465–473. https://doi.org/10.1016/j.compstruct.2009.04.024.
36. Şimşek, M. Bi-directional functionally graded materials (BDFGMs) for free and forced vibration of Timoshenko beams with various boundary conditions. *Compos. Struct.* **2015**, *133*, 968–978. https://doi.org/10.1016/j.compstruct.2015.08.021.
37. Hosseini SA, H.; Rahmani, O. Exact solution for axial and transverse dynamic response of functionally graded nanobeam under moving constant load based on nonlocal elasticity theory. *Meccanica* **2017**, *52*, 1441–1457. https://doi.org/10.1007/s11012-016-0491-2.
38. Ghadiri, M.; Rajabpour, A.; Akbarshahi, A. Non-linear forced vibration analysis of nanobeams subjected to moving concentrated load resting on a viscoelastic foundation considering thermal and surface effects. *Appl. Math. Model.* **2017**, *50*, 676–694. https://doi.org/10.1016/j.apm.2017.06.019.
39. Barati, M.R.; Shahverdi, H. Small-scale effects on the dynamic response of inhomogeneous nanobeams on elastic substrate under uniform dynamic load. *Eur. Phys. J. Plus* **2017**, *132*, 167. https://doi.org/10.1140/epjp/i2017-11441-9.
40. Zhang, Q.; Liu, H. On the dynamic response of porous functionally graded microbeam under moving load. *Int. J. Eng. Sci.* **2020**, *153*, 103317. https://doi.org/10.1016/j.ijengsci.2020.103317.
41. Liu, H.; Zhang, Q.; Ma, J. Thermo-mechanical dynamics of two-dimensional FG microbeam subjected to a moving harmonic load. *Acta Astronaut.* **2021**, *178*, 681–692. https://doi.org/10.1016/j.actaastro.2020.09.045.
42. Hosseini, S.A.; Rahmani, O.; Bayat, S. Thermal effect on forced vibration analysis of FG nanobeam subjected to moving load by Laplace transform method. *Mech. Based Des. Struct. Mach.* **2021**, 1–20. https://doi.org/10.1080/15397734.2021.1943671.
43. Abdelrahman, A.A.; Esen, I.; Daikh, A.A.; Eltaher, M.A. Dynamic analysis of FG nanobeam reinforced by carbon nanotubes and resting on elastic foundation under moving load. *Mech. Based Des. Struct. Mach.* **2021**, 1–24. https://doi.org/10.1080/15397734.2021.1999263.
44. Abdelrahman, A.A.; Esen, I.; Özarpa, C.; Eltaher, M.A. Dynamics of perforated nanobeams subject to moving mass using the nonlocal strain gradient theory. *Appl. Math. Model.* **2021**, *96*, 215–235. https://doi.org/10.1016/j.apm.2021.03.008.
45. Abdelrahman, A.A.; Esen, I.; Ozarpa, C.; Shaltout, R.; Eltaher, M.A.; Assie, A.E. Dynamics of perforated higher order nanobeams subject to moving load using the nonlocal strain gradient theory. *Smart Struct. Syst.* **2021**, *28*, 515–533. https://doi.org/10.12989/sss.2021.28.4.515.
46. Chung, K.L.; Tian, H.; Wang, S.; Feng, B.; Lai, G. Miniaturization of microwave planar circuits using composite microstrip/coplanar-waveguide transmission lines. *Alex. Eng. J.* **2022**, *61*, 8933–8942. https://doi.org/10.1016/j.aej.2022.02.027.
47. Eltaher, M.A.; Abdelrahman, A.A.; Esen, I. Dynamic analysis of nanoscale Timoshenko CNTs based on doublet mechanics under moving load. *Eur. Phys. J. Plus* **2021**, *136*, 705. https://doi.org/10.1140/epjp/s13360-021-01682-8.
48. Esen, I.; Abdelrahman, A.A.; Eltaher, M.A. On vibration of sigmoid/symmetric functionally graded nonlocal strain gradient nanobeams under moving load. *Int. J. Mech. Mater. Des.* **2021**, *17*, 721–742. https://doi.org/10.1007/s10999-021-09555-9.
49. Esen, I.; Eltaher, M.A.; Abdelrahman, A.A. Vibration response of symmetric and sigmoid functionally graded beam rested on elastic foundation under moving point mass. *Mech. Based Des. Struct. Mach.* **2021**, 1–25. https://doi.org/10.1080/15397734.2021.1904255.
50. Thongchom, C.; Roodgar Saffari, P.; Roudgar Saffari, P.; Refahati, N.; Sirimontree, S.; Keawsawasvong, S.; Titotto, S. Dynamic response of fluid-conveying hybrid smart carbon nanotubes considering slip boundary conditions under a moving nanoparticle. *Mech. Adv. Mater. Struct.* **2022**, 1–14. https://doi.org/10.1080/15376494.2022.2051101.
51. Akbaş, Ş.D.; Ersoy, H.; Akgöz, B.; Civalek, Ö. Dynamic analysis of a fiber-reinforced composite beam under a moving load by the Ritz method. *Mathematics* **2021**, *9*, 1048. https://doi.org/10.3390/math9091048.
52. Rajasekaran, S.; Khaniki, H.B. Size-dependent forced vibration of non-uniform bi-directional functionally graded beams embedded in variable elastic environment carrying a moving harmonic mass. *Appl. Math. Model.* **2019**, *72*, 129–154. https://doi.org/10.1016/j.apm.2019.03.021.
53. Attia, M.A.; Mahmoud, F.F. Modeling and analysis of nanobeams based on nonlocal-couple stress elasticity and surface energy theories. *Int. J. Mech. Sci.* **2016**, *105*, 126–134. https://doi.org/10.1016/j.ijmecsci.2015.11.002.
54. Attia, M.A. On the mechanics of functionally graded nanobeams with the account of surface elasticity. *Int. J. Eng. Sci.* **2017**, *115*, 73–101. https://doi.org/10.1016/j.ijengsci.2017.03.011.
55. Yang, T.; Tang, Y.; Li, Q.; Yang, X.D. Nonlinear bending, buckling and vibration of bi-directional functionally graded nanobeams. *Compos. Struct.* **2018**, *204*, 313–319. https://doi.org/10.1016/j.compstruct.2018.07.045.
56. Reddy, J.N.; Chin, C.D. Thermomechanical analysis of functionally graded cylinders and plates. *J. Therm. Stress.* **1998**, *21*, 593–626. https://doi.org/10.1080/01495739808956165.

57. Naghavi, M.; Sarrami-Foroushani, S.; Azhari, F. Bending analysis of functionally graded sandwich plates using the refined finite strip method. *J. Sandw. Struct. Mater.* **2022**, *24*, 448–483. https://doi.org/10.1177/1099636221102.
58. Nguyen, T.H.; Niiranen, J. Nonlocal continuum damage modeling for functionally graded plates of third-order shear deformation theory. *Thin-Walled Struct.* **2021**, *164*, 107876. https://doi.org/10.1016/j.tws.2021.107876.
59. Abo-bakr, R.M.; Shanab, R.A.; Attia, M.A. Multi-objective optimization for lightweight design of bi-directional functionally graded beams for maximum frequency and buckling load. *Compos. Struct.* **2021**, *278*, 114691. https://doi.org/10.1016/j.compstruct.2021.114691.
60. Gholami, R.; Ansari, R. Nonlinear resonance responses of geometrically imperfect shear deformable nanobeams including surface stress effects. *Int. J. Non-Linear Mech.* **2017**, *97*, 115–125. https://doi.org/10.1016/j.ijnonlinmec.2017.09.007.
61. Reddy, J.N. A simple higher-order theory for laminated composite plates, *ASME J. Appl. Mech.* **1984**, *51*, 745–752. https://doi.org/10.1115/1.3167719.
62. Kong, S. A review on the size-dependent models of micro-beam and micro-plate based on the modified couple stress theory. *Arch. Comput. Methods Eng.* **2022**, *29*, 1–31. https://doi.org/10.1007/s11831-021-09567-w.
63. Al-Basyouni, K.S.; Tounsi, A.; Mahmoud, S.R. Size dependent bending and vibration analysis of functionally graded micro beams based on modified couple stress theory and neutral surface position. *Compos. Struct.* **2015**, *125*, 621–630. https://doi.org/10.1016/j.compstruct.2014.12.070.
64. He, X.T.; Zhang, M.Q.; Pang, B.; Sun, J.Y. Solution of the Thermoelastic Problem for a Two-Dimensional Curved Beam with Bimodular Effects. *Mathematics* **2022**, *10*, 3002. https://doi.org/10.3390/math10163002.
65. Attia, M.A.; Mohamed, S.A. Nonlinear thermal buckling and postbuckling analysis of bidirectional functionally graded tapered microbeams based on Reddy beam theory. *Eng. Comput.* **2022**, *38*, 525–554. https://doi.org/10.1007/s00366-020-01080-1.
66. Yang, F.A.C.M.; Chong, A.C.M.; Lam, D.C.C.; Tong, P. Couple stress based strain gradient theory for elasticity. *Int. J. Solids Struct.* **2002**, *39*, 2731–2743. https://doi.org/10.1016/S0020-7683(02)00152-X.
67. Park, S.K.; Gao, X.L. Bernoulli–Euler beam model based on a modified couple stress theory. *J. Micromech. Microeng.* **2006**, *16*, 2355. https://doi.org/10.1088/0960-1317/16/11/015.
68. Li, Z.; He, Y.; Lei, J.; Guo, S.; Liu, D.; Wang, L. A standard experimental method for determining the material length scale based on modified couple stress theory. *Int. J. Mech. Sci.* **2018**, *141*, 198–205. https://doi.org/10.1016/j.ijmecsci.2018.03.035.
69. Nguyen, D.K.; Nguyen, Q.H.; Tran, T.T.; Bui, V.T. Vibration of bi-dimensional functionally graded Timoshenko beams excited by a moving load. *Acta Mech.* **2017**, *228*, 141–155. https://doi.org/10.1007/s00707-016-1705-3.
70. Songsuwan, W.; Pimsarn, M.; Wattanasakulpong, N. Dynamic responses of functionally graded sandwich beams resting on elastic foundation under harmonic moving loads. *Int. J. Struct. Stab. Dyn.* **2018**, *18*, 1850112. https://doi.org/10.1142/S0219455418501122.
71. Ebrahimi, F.; Salari, E. Thermal buckling and free vibration analysis of size dependent Timoshenko FG nanobeams in thermal environments. *Compos. Struct.* **2015**, *128*, 363–380. https://doi.org/10.1016/j.compstruct.2015.03.023.
72. Dehrouyeh-Semnani, A.M.; Mostafaei, H.; Dehrouyeh, M.; Nikkhah-Bahrami, M. Thermal pre-and post-snap-through buckling of a geometrically imperfect doubly-clamped microbeam made of temperature-dependent functionally graded materials. *Compos. Struct.* **2017**, *170*, 122–134. https://doi.org/10.1016/j.compstruct.2017.03.003.
73. Olsson, M. On the fundamental moving load problem. *J. Sound Vib.* **1991**, *145*, 299–307. https://doi.org/10.1016/0022-460X(91)90593-9.
74. Dimitrovová, Z.; Varandas, J.N. Critical velocity of a load moving on a beam with a sudden change of foundation stiffness: Applications to high-speed trains. *Comput. Struct.* **2009**, *87*, 1224–1232. https://doi.org/10.1016/j.compstruc.2008.12.005.